Research Department

Technical Report No. 75

An improved land surface parametrization scheme in the ECMWF model and its validation

by

Pedro Viterbo and Anton C M Beljaars*

* KNMI, The Netherlands

Accepted for publication by Journal of Climate

March, 1995

Abstract

A new version of the ECMWF land surface parametrization scheme is described. It has four prognostic layers in the soil for temperature and soil moisture, with a free drainage and a zero heat flux condition at the bottom as boundary condition. The scheme has been extensively tested in stand-alone mode with the help of long observational time series from three different experiments with different climatological regimes: FIFE in the USA, Cabauw in the Netherlands and ARME in Brazil. The emphasis is on seasonal time scales because it was felt that the main deficiencies in the old ECMWF land surface scheme were related to its capability of storing precipitation in spring and making it available for evaporation later in the year. It is argued that the stand-alone testing is particularly important because it allows one to isolate problems in the land surface scheme without having to deal with complicated interactions in the full three dimensional model.

1. INTRODUCTION

The parametrization of land surface processes in numerical weather prediction (NWP) or climate general circulation models (GCMs) is important for a number of reasons. First of all, the sensible and latent heat fluxes at the surface are the lower boundary conditions for the heat and moisture equations in the atmosphere. Given the correct radiative forcing at the surface, the land surface schemes are also largely responsible for the quality of model produced near surface weather parameters, such as screen level temperature and dew point, and low level cloudiness. Furthermore, the surface conditions need to be such as to provide the adequate feedback mechanisms for the other physical processes in the atmosphere: low level cloudiness influences the surface radiative balance, sensible heat and latent heat fluxes influence the boundary layer exchanges and the intensity of the moist convective processes. Finally, the correct partitioning between sensible and latent heat fluxes determines the soil wetness, which acts as one of the forcings of low frequency atmospheric variability (*Delworth and Manabe*, 1988, 1989; *Milly and Dunne*, 1994).

Processes at the soil-vegetation-atmosphere interface, and their impact on GCMs are reviewed in *Mintz* (1984) and *Garratt* (1993). First studies on the role of soil water (*Namias*, 1958) led to the development of the so-called "bucket model" for evaporation and computation of surface runoff (*Manabe*, 1969). With the work of *Deardorff* (1978), the attention has somehow been switched from the role of soil water as a *slow* variable in the climatic system to the role played by the vegetation cover in determining the rate of transpiration. Many of the schemes used today in GCMs (e.g. *Dickinson et al*, 1986; *Sellers et al*, 1986; *Abramapoulos et al*, 1989; *Noilhan and Planton*, 1989) mimic the effect of plant physiology in using, e.g., the amount of photosynthetic active solar radiation and the availability of water in the root zone to regulate the opening and closing of leaf stomata, thus controlling the flow of water from the soil into the atmosphere and defining the transpiration rate. The concept of stomatal conductance as a product of different stress functions (*Jarvis*, 1976) is central to all the above models. On the other hand, many GCMs incorporate an interception reservoir, collecting rain and re-evaporating at the potential rate (*Rutter et al*, 1972). Most of these studies concentrate on short time scales, e.g the diurnal cycle and the drying of the interception reservoir. This paper addresses the longer time scales.

The surface scheme operational in the ECMWF model until July 1993 was based on the heat and water budget of two active soil layers plus an additional surface layer underneath, acting as a "climate layer" (*Blondin*, 1991). The model also incorporated a vegetation based evaporation scheme, of the kind described above, and an interception reservoir. Comparisons of model results with FIFE field data (*Betts et al*, 1993), and verification of the daily forecast products, identified a number of problems associated with the surface/boundary layer scheme: a) surface evaporation too large in wet conditions and too small in dry

conditions, b) large positive bias in the atmospheric surface temperature in Summer, during day time, c) land hydrology inaccurate and dominated excessively by the prescribed "climate fields".

An improved surface model, suitable for use with NWP models and climate models, has been developed, in order to tackle the problems referred to above. Special attention has been devoted to an accurate representation of the soil water transfer at all time scales, since it was felt that this was one of the major causes of the systematic errors described above. Comparison of results of the old model with FIFE observations, referred above, suggested improvements in three areas of sub-surface hydrology and evaporation: a) First, a mechanism is necessary to get precipitation rapidly into the ground, where it can be stored, b) Second, sufficient storage is needed to represent several weeks of evaporation without rain; c) Third, seasonal and interannual memory of soil moisture anomalies needs deep predicted reservoirs. The idea behind this model development has been to improve on documented deficiencies, but on the other hand to keep the model as simple as possible. This has resulted in a model that has many aspects of more complex schemes such as BATS and SiB (*Dickinson et al*, 1986; *Sellers et al*, 1986), but does not have the many geographically dependent parameters as soil type, vegetation type etc. Single column validation of the model against results of field experiments has been a key part of the model development, and has provided most of the insight for isolating relevant mechanisms. The purpose of this paper is to present the new model, and the results of comparison of the old and new model with observations. The emphasis is on validation with continuous long single column runs of the surface model forced by near surface observed weather parameters, in view of the long time scales of the problems involved. In this way we validate the land surface scheme in isolation from other model deficiencies and avoid complicated feedbacks from the atmospheric forcing.

In addition to the single column simulations, multiyear runs with the full three-dimensional model were carried out at T63L31 resolution. The purpose of the GCM simulations is threefold: i) They act as a surrogate of several years of data assimilation, an experiment that is too demanding on computer resources, and therefore cannot be done; ii) They show that there is no dramatic model drift, both models producing a not unreasonable climate for those locations; iii) They reinforce the idea that one-column validation is essential for deciding on the advantages of the new over the old scheme. The surface energy budget of these integrations is studied for the same locations as the ones used in the single column validation. Biases tend to be large, but model feedbacks, and deficiencies in the atmospheric forcing, make it difficult to draw firm conclusions about the origins of these biases. For this reason the stand-alone tests are very important to identify problems in the surface component of the model. With a well tested land-surface scheme we are in a better position to tackle problems in other components of the model parametrization.

Section 2 of the paper describes the new model. The soil heat and water budget are discussed, and the choice of particular options and model constants is justified. Section 3 describes the single column simulations for different observational time series. Three datasets are used. Cabauw (in the Netherlands) was chosen for its relatively simple hydrology. FIFE (First ISLSCP Field Experiment, with ISLSCP for International Satellite Land-Surface Climatology Project) shows the model performance in the transition from a wet Spring to a sequence of dry spells and precipitation events in Summer. Finally, comparison with ARME (Amazonian Rainforest Meteorological Experiment) data highlights the properties of the new model for tropical eco-systems. Section 4 describes the results of the multi-year integrations with the old and the new parametrization in the full three- dimensional model. Conclusions are presented in section 5, stressing the importance of a correct treatment of weekly to seasonal time scales in soil moisture. The differences between the old model and new model are summarized in the Appendix.

2. THE NEW ECMWF SURFACE MODEL: MODEL DESCRIPTION

2.1 **Motivation**

In the absence of snow in the ground, the soil heat and water budget are represented by two partial differential equations. The top boundary conditions are the net heat flux and infiltration minus evaporation for the heat and water budget, respectively. The total soil depth and the spatial discretization chosen must be such that all time scales relevant to the atmospheric forecast problem - ranging form the diurnal cycle up to the seasonal time scales -are adequately represented. The model described below has four layers in the vertical plus a thin interception layer for the water budget, and a "layer" with no heat capacity at the top, in instantaneous equilibrium with its forcing, to define the skin temperature. Bottom boundary conditions are zero heat flux and free drainage. Fig 1 summarizes the main features of the model.

2.2 **The soil heat budget**

The soil heat transfer is assumed to obey the following Fourier law of diffusion

$$(\rho C)_s \frac{\partial T}{\partial t} = \frac{\partial}{\partial z}\left[\lambda_T \frac{\partial T}{\partial z}\right] \tag{1}$$

where $(\rho C)_s$ is the volumetric soil heat capacity (units $Jm^{-3}K^{-1}$), T is the soil temperature (units K), z is the vertical coordinate - distance from the surface, positive downwards - in m, and λ_T is the thermal conductivity (units $Wm^{-1}K^{-1}$). The above equation assumes that heat fluxes are predominantly in the vertical direction, the effects of phase changes in the soil and the heat transfer associated to the vertical movement of water in the soil can be neglected (*de Vries*, 1975), and that the effects of hysteresis can be neglected (*Milly*, 1982).

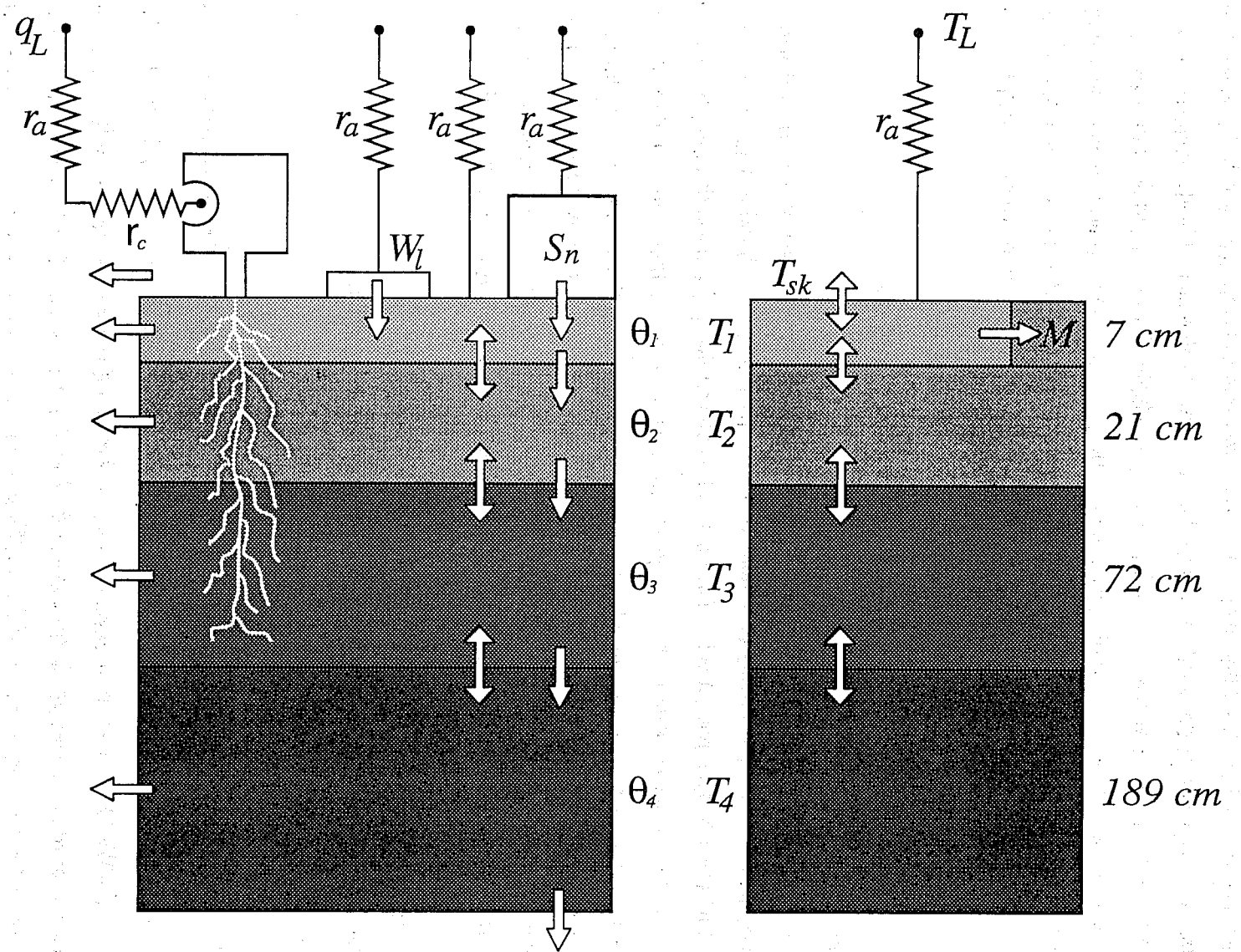

Fig 1 Schematic description of the structure of the land surface model. Double arrows mean diffusivity processes, single arrows represent "drainage-like" terms (soil drainage, snow melting and throughfall/top infiltration for the skin reservoir), horizontal arrows represent surface and sub-surface runoff (bottom drainage is lost to the model and is therefore a runoff term). The bottom value of the resistance network for evaporation is $q_{sat}(T_{sk})$, except for the bare ground, where a relative humidity α is assumed (see eq (19)). In the heat transfer panel, the snow mass replaces a portion of the first model layer (M), and the horizontal arrow represents heat exchanges due to melting.

The solution of the partial differential equation (1) needs the specification of boundary conditions. The top boundary condition is the net heat flux at the surface - sum of the radiative, latent and sensible heat fluxes. We will assume no heat flux of energy at the lower boundary. This is an acceptable approximation, provided that the total soil depth is large enough for the time scales in which we are interested or, in other terms, the bottom of the soil is specified at a depth where the amplitude of the soil heat wave is a negligible fraction of its surface amplitude (see *de Vries*, 1975, and subsection below).

2.2.1 *Discretization and choice of parameters*

For the solution of equation (1) the soil is discretized in four layers, of depths D_i, (i=1,2,3,4). Defining the temperatures at full layers and the heat fluxes at half layers (the interfaces between two adjacent layers):

$$\frac{(\rho C)_i}{\Delta t}(T_i^{n+1} - T_i^n) = -\frac{(G_{i,b} - G_{i,t})}{D_i} \qquad i=1,2,3,4 \tag{2}$$

where Δt is the timestep in seconds, and $G_{i,b}$ and $G_{i,t}$ are the heat fluxes (positive downwards, units Wm^{-2}) at the bottom and top of layer i respectively, defined as:

$$\begin{aligned} G_{i,b} &= -\lambda_{T,i+1/2}\frac{T_{i+1}^n - T_i^{n+1}}{0.5(D_i + D_{i+1})} \qquad i=1,2,3 \\ G_{i,t} &= -\lambda_{T,i-1/2}\frac{T_i^{n+1} - T_{i-1}^n}{0.5(D_{i-1} + D_i)} \qquad i=2,3,4 \end{aligned} \tag{3}$$

In equations (2) and (3) the superscript n identifies variables at time $n\Delta t$. The above equations correspond to a "locally implicit" method: the equations are decoupled because time $(n+1)\Delta t$ is only present for layer i in the equation (2). Note that the method is non-conservative: the flux seen by layer i from layer $i-1$ is not identical to minus the flux seen by layer $i-1$ coming from layer i. In the simulations performed, the difference between the two fluxes is less than 0.1%.

The boundary condition at the top and at the bottom are

$$\begin{aligned} G_{1,t} &= \Lambda_{sk}(T_{sk} - T_1) \\ G_{4,b} &= 0 \end{aligned} \tag{4}$$

$G_{1,t}$ is the ground heat flux at the interface soil-atmosphere interface. For the definition of the skin temperature, T_{sk}, and the numerical value of the empirical coefficient Λ_{sk}, see next subsection.

The volumetric heat capacity is assumed constant, with value $2.19 \cdot 10^6$ $Jm^{-3}K^{-1}$ (see Table 1 for a list of constants used by the model). The heat conductivity, depends on the soil water content following *McCumber and Pielke* (1981):

$$\lambda_T(\theta) = a\|\psi_{sat}\|^{-1/\log 10}\left(\frac{\theta_{sat}}{\theta}\right)^{-b/\log 10} \quad \theta > \theta_\lambda$$
$$= \lambda_{min} \quad \theta \le \theta_\lambda \tag{5}$$

D_1	Depth of soil layer 1	0.07 m
D_2	Depth of soil layer 2	0.21 m
D_3	Depth of soil layer 3	0.72 m
D_4	Depth of soil layer 4	1.89 m
R_1	Fraction of roots in layer 1	0.33
R_2	Fraction of roots in layer 2	0.33
R_3	Fraction of roots in layer 3	0.33
R_4	Fraction of roots in layer 4	0
ρC_s	Volumetric soil heat capacity	$2.19\ 10^6$ $Jm^{-3}K^{-1}$
θ_{sat}	Soil moisture at saturation	0.472 $m^{-3}m^{-3}$
θ_{cap}	Soil moisture at field capacity	0.323 $m^{-3}m^{-3}$
θ_{pwp}	Soil moisture at permanent wilting point	0.171 $m^{-3}m^{-3}$
Ψ_{sat}	Matric potential at saturation	-0.338 m
γ_{sat}	Hydraulic conductivity at saturation	$4.57\ 10^{-4}$ ms^{-1}
a	Clapp and Hornberger soil parameter	3.8
b	Clapp and Hornberger soil parameter	6.04
L_f	Leaf area index	4
ϵ	Surface emissivity	0.996
W_{max}	Maximum water amount on single leaf	0.0002 m
r_{smin}	Minimum stomatal resistance of single leaf	240 sm^{-1}
Λ_{sk}	Skin layer "conductivity"	7 $Wm^{-2}K^{-1}$
k	Heterogeneity factor for convective precipitation	0.5
c_i	Interception efficiency	0.25

Table 1 Parameters in the land surface scheme

b is the Clapp and Hornberger exponent (*Clapp and Hornberger*, 1978; *Cosby et al*, 1984), a comes from the fact that we use different units from McCumber and Pielke and is a constant independent of soil type (a=3.8), θ is the volumetric soil water content (units m^3/m^3) and ψ is the matric potential, representing the work required to extract water from the soil against capillarity and gravity (units m of water). λ_{min} is the minimum value of heat conductivity (0.171 $Wm^{-1}K^{-1}$); θ_λ is the threshold value of soil moisture that assures first-order continuity of the functional dependency in (5). Subscript *sat* indicates values at saturation: see section 2d below for the choice of numerical values for b, ψ_{sat} and θ_{sat}. Equation (5) is applied to layer i and layer $i+1$, and $\lambda_{i+½}$ is taken as the maximum of the two values. This choice of "upstream" values of heat conductivity minimizes truncation errors associated with the representation of large gradients in soil water with a coarse soil grid (*Mahrt and Pan*, 1984).

The depths of the soil layers are chosen in an approximate geometric relation, as suggested in *Deardorff* (1978):

$D_1 = 0.07$ m, $D_2 = 0.21$ m, $D_3 = 0.72$ m, $D_4 = 1.89$ m

Warrilow et al (1986) have shown that 4 layers are enough for representing correctly all time scales from one day to one year. With the numerical values of the heat capacity and soil depths, we have analyzed the amplitude and phase response of the numerical solution of equation (1) for typical values of soil moisture in equation (5), and for harmonic forcings at the surface with periods ranging from half a day to 2 years. The discretization of equation (1) has two consequences: i) For each soil moisture value, there is a quasi-resonant period, related to the total depth of the soil, and to the no-flux boundary condition; ii) There are other relevant periods, linked to the ratio of the depths of the soil layers (see *Dickinson*, 1988). For the above choice of depths, and the thermal properties defined by equation (5), the analysis of Warrilow et al indicates an error in the numerical solution of less than 20% in amplitude and 5% in phase for forcing periods between one day and one year.

2.2.2 *The skin temperature*

Above the soil layer we assume a skin layer with zero heat capacity, representing the effect of vegetation and litter on bare soil in isolating the radiative heating from the underlying soil. The skin layer has been introduced to reduce the phase error in the diurnal cycle of sensible, latent and ground heat flux and to reduce the magnitude of the ground heat flux (*Betts et al*, 1993). The skin temperature is defined with the help of "conductivity" Λ_{sk} which relates the ground heat flux to the difference between T_{sk} and T_1 (eq. 4). For $\Lambda_{sk} = 7$ $Wm^{-2}K^{-1}$, *Beljaars and Betts* (1993) found that the sensible and latent heat flux of the model were in phase with FIFE observations, and the diurnal cycle of the ground heat flux was within ± 25% of the observed values. Because the skin layer has no heat capacity, the surface energy balance equation can

be written as

$$(1-\alpha)R_S + R_T - \epsilon\sigma T_{sk}^4 + H + L\cdot E = \Lambda_{sk}(T_{sk} - T_1) \tag{6}$$

where R_S and R_T are the surface downward radiative fluxes, H is the sensible heat and E is the surface evaporation. All fluxes are positive downwards, the energy fluxes have units Wm^{-2}, E in $kgm^{-2}s^{-1}$. α is the surface albedo, ϵ is the surface emissivity, σ is the Stefan-Boltzman constant ($Wm^{-2}K^{-4}$) and L is the latent heat of evaporation (Jkg^{-1}).

To parametrize H and E we use transfer coefficients between the surface (skin) and the lowest atmospheric model level expressed as a function of the Obukhov length (*Beljaars and Viterbo*, 1994). The advantage of using the Obukhov length, instead of a simpler formulation in terms of a Richardson number (*Louis*, 1979), is that the empirical stability functions can be specified as they have been measured, and the surface roughness lengths for momentum, heat and moisture can be chosen independently; we shall take the roughness length for heat equal to that for moisture. In this formulation one must use an iterative process to convert the Richardson number into an Obukhov length every time step. The sensible heat flux and the evaporative flux can be written as:

$$\begin{aligned} H &= \rho C_H \|u_L\| (C_p T_L + g z_L - C_p T_{sk}) \\ E &= \rho C_H \|u_L\| [a_L q_L - a_s q_{sat}(T_{sk}, p_s)] \\ \|u_L\|^2 &= U^2 + V^2 + w_*^2, \qquad w_* = \left(z_i \frac{g}{T_v} \overline{w'\theta_v'}\right)^{1/3} \end{aligned} \tag{7}$$

In the above expressions ρ is the air density (kgm^{-3}), U, V, T_L and q_L are the wind speed components, temperature and specific humidity at the lowest model level, C_p the heat capacity of the air at constant pressure, g is the acceleration of gravity, z_L is the height of the lowest model level, p_s is the surface pressure (Pa), w_* is the free convection velocity, z_i is the boundary layer height T_v is the virtual temperature and $\overline{w'\theta_v'}$ is the virtual temperature flux. For the definition of the exchange coefficient C_H as a function of the Obukhov length see *Beljaars and Holtslag* (1991) and *Beljaars and Viterbo* (1994). a_L and a_s are coefficients implicitly defined when the evaporation scheme is further detailed (see section 2c below). The free convection velocity has been added in the transfer law of equation (7) to ensure a proper free convection limit (see *Beljaars*, 1995). Since only the order of magnitude of z_i matters, a constant value of 1000 m has been selected.

By inserting (7) into (6) we obtain a non-linear equation for T_{sk}. Because of the short time scales associated with the skin temperature, typically of the order of the time step used, we have to be careful when solving this equation. We have therefore chosen to solve for the skin temperature together with the solution of the vertical diffusion in the boundary layer. In solving the tri-diagonal system for the boundary layer (*Richtmyer and Morton*, 1967), we will have N+1 layers, where N is the number of model levels in the atmosphere. The additional N+1 layer, representing the balance of skin temperature, is obtained by substituting (7) into (6) and linearizing the upward thermal radiation, sensible heat, evaporation and $q_L(T_{sk})$.

2.2.3 *Time scales*

To provide an insight into the time scales associated with each layer we will rewrite (2) and (3) in the following way

$$\frac{\partial T_i}{\partial t} = S_i + \frac{T_{i-1} - T_i}{\tau_i{}^u} + \frac{T_{i+1} - T_i}{\tau_i{}^d} \tag{8}$$

where S_i represents the effect of any fluxes at the boundaries (S_i=0, for i=2,3,4). τ_i^u and τ_i^d represent time scales of interaction with the layer above and the layer below respectively. They depend on the soil depths, the heat capacity and the heat diffusivity, hence the soil moisture. They increase with layer depth and decrease with soil wetness. For any given layer, the interactions with the layer below have longer time scales than the interactions with the layer above. Table II shows the values of τ for the 4 soil layers; they were obtained using equation (5), in combination with the values of the soil depths. Each column represents a value of soil moisture, ranging from permanent wilting point value (0% of availability) to field capacity (100% of availability): see section 2c for a full explanation of the meaning of these quantities. For each layer, two values are given: the upper value gives the upward time scale, and the lower value the downward scale. Time scales range from fractions of a day to around 150 days, increasing from top to bottom and decreasing with soil moisture. In qualitative terms, the first layer represents the diurnal cycle, the second layer represents variations between one day and one week, the third layer represents variations between one week and one month, while the fourth layer represents variations with time scales larger than one month. Notice that the behaviour for very short time scales (less than a few hours) is controlled by the skin temperature and its ability to adjust instantaneously to variations in the surface radiative forcing; the values in Table II do not include this effect.

	0 %	33 %	67 %	100 %
1 upwards	-	-	-	-
1 downwards	0.6	0.3	0.2	0.1
2 upwards	1.8	0.9	0.5	0.3
2 downwards	5.8	3.0	1.7	1.1
3 upwards	19.9	10.2	5.9	3.8
3 downwards	55.8	28.6	16.5	10.6
4 upwards	146.4	75.0	43.4	27.9
4 downwards	-	-	-	-

Table 2 Temperature time scale (in days) associated to each layer, dependent on soil moisture (percent of maximum availability). See text for an explanation of the different quantities.

2.3 **Evaporation**

For the purpose of computing evaporation, we conceptually divide every snow free grid-box over land in three fractions (*Blondin*, 1991):

i) C_l Fraction covered by the interception reservoir

ii) $(1-C_l)*C_v$ Dry vegetation fraction

iii) $(1-C_l)*(1-C_v)$ Dry bare soil fraction

A different evaporation rate is computed for each fraction, and the total evaporation (E, $kgm^{-2}s^{-1}$) is a weighted sum of the three components, E_l, E_v, E_g respectively:

$$E = C_l E_l + (1-C_l)C_v E_v + (1-C_l)(1-C_v)E_g \tag{9}$$

The geographical distribution of the vegetation fraction, C_v, is prescribed following *Wilson and Henderson-Sellers* (1985), with a correspondence table, relating each vegetation type to a fixed cover, based on *Warrilow et al* (1986).

2.3.1 *Evaporation from the interception reservoir*

The interception reservoir represents the reservoir collecting water by interception of precipitation and collection of dew. The fraction of the grid box covered by the interception reservoir is given by

$$C_l = \min(1, \frac{W_l}{W_{lmx}}) \tag{10}$$

where W_l is the water content of the interception reservoir (m of water), W_{lmx} is the maximum value for the intercepted water, given by (see *Dickinson*, 1984; *Noilhan and Planton*, 1989)

$$W_{lmx} = [C_v L_f + (1-C_v)] \cdot W_{\max} \tag{11}$$

L_f is the leaf area index with a global value (L_f=4) as in the old ECMWF model (*Blondin*, 1991). Its value determines the size of the interception reservoir; the simulations with ARME (see section 3c) seem to justify that value for that particular place. If reliable information about this quantity (*Carlson*, 1991) is made available timely, a NWP model could use a different global distribution say every week or every fortnight. W_{max} is a constant, corresponding to the maximum water in a single leaf or that can stay as a film over bare ground (W_{max}=0.0002 m). *Deardorff* (1978) argues that, instead of a linear dependency of the interception reservoir fraction on its water content, one should use a fractional power a, a<1. Using such a power would produce a faster depletion of intercepted water after an such as collection of dew or interception of rainfall has taken place. With a=1, as in equation (10) the intercepted water could possibly never quite disappear because the decrease would be exponential for a fixed value of potential evaporation (see section 2d below, on the evolution of the content of the interception reservoir). In practice we found no problems by assuming a=1.

The interception reservoir evaporates at the potential rate

$$E_l = \frac{\rho}{r_a}(q_L - q_{sat}(T_{sk}, p_s)) \tag{12}$$

r_a is the aerodynamic resistance (sm^{-1}). By comparison of (12) and (7),

$$r_a = \frac{1}{C_H \|u_L\|} \tag{13}$$

2.3.2 *Dry vegetation evaporation*

The dry vegetation transpires at the rate

$$E_v = \frac{\rho}{r_a + r_c}(q_L - q_{sat}(T_{sk}, p_s)) \tag{14}$$

The canopy resistance, r_c, (sm^{-1}), is given by a product of a minimum value and a number of limiting factors, depending on environmental conditions (*Jarvis*, 1976; see also review by *Dickinson et al*, 1990):

$$r_c = \frac{r_{smin}}{L_f} f_1(PAR) f_2(\bar{\theta}) \tag{15}$$

PAR is the photosynthetically active radiation (PAR=0.55(1-α)R_S), r_{smin} is the minimum stomatal resistance of a single leaf (r_{smin}= 240 sm^{-1}), θ is a mean soil moisture in the root zone, and f_1, f_2 are stress functions for the photosynthetically active radiation and the soil wetness in the root zone, respectively. We follow *Sellers* (1985) in adopting:

$$\frac{1}{f_1(PAR)} = 1 - a_1 \log \frac{a_2 + PAR}{a_3 + PAR} \tag{16}$$

For a particular site, a_1, a_2 and a_3 can be related to canopy properties (see *Sellers*, 1985). Equation (16) is based on an integration across the canopy of the conductances (inverse of resistances) of individual horizontal leaves acting in parallel. The values of *Blondin* (1991) were used (a_1=0.19, a_2=1128 Wm^{-2}, a_3=30.8 Wm^{-2}), since no particular problem was felt to exist in f_1 used in the old model.

As noted by *Dickinson et al* (1990) there is no agreement among modellers for the water stress dependence, and there is very little experimental evidence to support any of the different model choices available (see for instance *Sellers et al*, 1986; *Xue et al*, 1991, for SiB and SSiB; *Wilson et al*, 1987, for BATS and *Abramopoulos et al*, 1988, for GISS). Based on its simplicity, we have adopted the moisture content approach of *Noilhan and Planton* (1989), rather than a soil water potential dependence (as in SiB, SSiB, BATS, and GISS):

$$\frac{1}{f_2(\bar{\theta})} = \begin{cases} 0 & \bar{\theta} < \theta_{pwp} \\ \dfrac{\bar{\theta} - \theta_{pwp}}{\theta_{cap} - \theta_{pwp}} & \theta_{pwp} < \bar{\theta} < \theta_{cap} \\ 1 & \bar{\theta} > \theta_{cap} \end{cases} \tag{17}$$

f_1 and f_2 are set to 1 in case of dew deposition ($q_L > q_{sat}(T_{sk}, p_s)$). The specification of the soil moisture at the root zone, θ, in equation (17), in terms of the soil water contents of the model layers, is probably more important than the functional relationship chosen. The datasets available (see later for ARME, and FIFE, and *Goutorbe et al*, 1989, for HAPEX-MOBILHY) indicate a depletion of soil moisture at the top after a precipitation event, with a highly curved soil moisture profile. We have adopted

$$\bar{\theta} = R_1\theta_1 + R_2\theta_2 + R_3\theta_3 \tag{18}$$

with $R_1 = R_2 = R_3 = 0.33$, specifying the vertical distribution of the roots in the soil. Note that since the soil depths follow a geometric series, the root profile adopted implies a root density exponentially decreasing with depth. For further discussion in the root profile, and the absence of roots in the fourth layer, see section 2d below.

Equation (15) does not specify any dependence of stress on the saturation deficit or temperature, as opposed to, e.g., SiB or *Noilhan and Planton* (1989). The specification of both the above stresses is highly species

dependent. Since the vegetation in the model is only specified by its fractional cover (there is only one vegetation type everywhere), it is difficult to include effects that depend strongly on species.

2.3.3 *Bare ground evaporation*

Soil (bare ground) evaporation is due to a combination of two physical processes (*Kondo et al*, 1990): i) Molecular diffusion from the water trapped in the pores of the soil matrix up to the land surface level, defined by the humidity roughness length, z_0q (see *Brutsaert*, 1982); ii) laminar and turbulent exchange in the air between z_0q and screen level height. Process i) is clearly dependent on the relative humidity of the air pores adjacent to the water in the soil matrix, in itself a function of the soil temperature close to the pores. In dry situations this relative humidity in the pores has strong vertical gradients in the first few mm of soil.

Mahfouf and Noilhan (1991) made a comparative study of several formulations of evaporation over bare ground. Given the above description it is not surprising that most methods reviewed are very sensitive to the top soil discretization of NWP models. The methods presently available were classified in bulk parametrization approaches (α- type and β- type, following *Kondo et al*, 1990) and threshold methods. The β- methods seem to overestimate the night time dew deposition, although the observation methods were not accurate enough to draw firm conclusions (*Mahfouf and Noilhan*, 1991). We have adopted an α- method modelling the evaporation as a bulk transfer of water vapour between z_0q (assumed at relative humidity α, where α depends on the soil wetness of the top model layer), and the lowest atmospheric model level:

$$E_g = \frac{\rho}{r_a}[q_L - \alpha\, q_{sat}(T_{sk}, p_s)] \tag{19}$$

$$\alpha = \begin{cases} 0.5\left[1 - \cos\left(\frac{\pi}{1.6}\frac{\theta_1}{\theta_{cap}}\right)\right] & \theta_1 < \theta_{cap} \\ 1 & \theta_1 \geq \theta_{cap} \end{cases} \tag{20}$$

α=1 in case of dew deposition ($q_L > q_{sat}(T_{sk}, p_s)$). The factor 1.6 has been added to account for the difference between soil moisture at the surface (for which this parametrization has been designed) and θ_1, an averaged value over 7 cm depth. The factor is compatible with the results by *Mahrt and Pan* (1984), who studied the effect of vertical resolution on drying soil at a rate of 1 mm/hr.

2.4 The soil water budget

The vertical movement of water in the unsaturated zone of the soil matrix obeys the following equation (see *Hillel*, 1982; *Richards*, 1931; *Philip*, 1957; *Milly*, 1982, for the conditions under which equations (21) and

(22) are valid):

$$\rho_w \frac{\partial \theta}{\partial t} = -\frac{\partial F}{\partial z} + \rho_w S_\theta \tag{21}$$

ρ_w is the water density (kgm^{-3}), F is the water flux in the soil (positive downwards, $kgm^{-2}s^{-1}$), and S_θ is a volumetric source term ($m^3m^{-3}s^{-1}$), corresponding to root extraction. Using Darcy's law, F can be specified as:

$$F = -\rho_w(\lambda \frac{\partial \theta}{\partial z} - \gamma) \tag{22}$$

λ (m^2s^{-1}) and γ (ms^{-1}) are the hydraulic diffusivity and hydraulic conductivity, respectively.

Replacing (22) in (21), specifying $S_\theta = S_\theta(\theta,z)$, and defining parametric relations for λ and γ as a function of soil water, we obtain a partial differential equation for the soil moisture that can be numerically integrated if we provide the boundary conditions and the fluxes of water at the top and bottom of the soil. The top boundary condition is precipitation minus evaporation minus surface runoff. The bottom boundary condition is free drainage. *Abramopoulos et al* (1988) specify free drainage or no drainage, dependent on a comparison of a specified geographical distribution of bedrock depth, with a model derived water table depth. For the sake of simplicity, and to avoid the use of yet another global dataset, we simply assume no bedrock everywhere.

2.4.1 *Interception and the interception reservoir*

The interception reservoir is a thin layer on top of the soil/vegetation, collecting water by interception of rain and collection of dew, and evaporating at the potential rate. The water in the interception reservoir, W_l, obeys

$$\frac{\partial W_l}{\partial t} = \frac{(I + C_l E_1)}{\rho_w} \tag{23}$$

where $C_l E_l$ ($kgm^{-2}s^{-1}$) is the water evaporated by the interception reservoir (or dew collection, depending on its sign) and I ($kgm^{-2}s^{-1}$) is the interception, that fraction of precipitation that is collected by the interception reservoir and is later available for potential evaporation. Because the interception reservoir has a very small capacity (a maximum of 0.8 mm, see equation (11)), it can fill up or evaporate completely in one time step: special care has to be taken in order to avoid numerical problems when integrating equation (23). First, the evaporation contribution is considered; because $C_l E_l$ depends linearly on W_l (see equation (10)), an implicit version of the evaporating part of (23) is obtained by linearizing $C_l(W_l)E_l$:

$$\rho_w \frac{W_l^{n+1,1} - W_l^n}{\Delta t} = C_l(W_l^n)E_l + \frac{E_l}{W_{lmx}}(W_l^{n+1,1} - W_l) \quad (24)$$

where $W_l^{n+1,1}$ is the new value of interception reservoir content after the evaporation process is taken into account. Equation (24) guarantees non-negative results for $W_1^{n+1,1}$. Collection of dew is done in an explicit way, obtaining a new value $W_1^{n+1,1}$. A rate of evaporation (and collection of dew) effectively used by the interception reservoir, E_1^*, can be computed by comparing $W_1^{n+1,1}$ with ; this evaporation rate is deduced from the total evaporation, , and then used to force the soil (see section 2d below).

Interception is computed as the fraction of the precipitation flux that can be stored in the interception reservoir, the remaining part being throughfall:

$$I = \min(c_i C_v P^*, \rho_w \frac{W_{lmx} - W_l^{n+1,1}}{\Delta t}) \quad (25)$$

$P^*=P/k$ is a modified precipitation flux, computed by applying the heterogeneity assumption that precipitation only covers a fraction k of the grid-box, P is precipitation obtained from the atmospheric input, c_i is a coefficient of efficiency of interception of rain (c_i=0.25). The heterogeneity factor k is 0.5 for convective precipitation and 1 for large scale precipitation (*Viterbo and Illari*, 1994). Throughfall T ($kgm^{-2}s^{-1}$), an input for the soil reservoir, is

$$T = P - I \quad (26)$$

The interception reservoir model described in this section is probably the simplest water conserving formulation based on Rutter's original proposition (*Rutter et al*, 1972; *Rutter et al*, 1975). For more complicated formulations, still based on the Rutter concept, see for instance *Mahfouf and Jacquemin* (1989), or *Dolman and Gregory* (1992).

2.4.2 *Soil properties*

Integration of equations (21) and (22) requires the specification of hydraulic conductivity and diffusivity as a function of soil water content. *Mahrt and Pan* (1984) compare several formulations for different soil types. We have adopted the widely used parametric relations of *Clapp and Hornberger* (1978), see also *Cosby et al* (1984)

$$\gamma = \gamma_{sat}\left(\frac{\theta}{\theta_{sat}}\right)^{2b+3}$$

$$\lambda = \frac{b\gamma_{sat}(-\psi_{sat})}{\theta_{sat}}\left(\frac{\theta}{\theta_{sat}}\right)^{b+2} \qquad (27)$$

b is a non-dimensional exponent, γ_{sat} and ψ_{sat} are the values at saturation of hydraulic conductivity and matric potential, respectively. A minimum value is assumed for λ and γ, corresponding to permanent wilting point water content.

Cosby et al (1984) tabulate best estimates of b, ψ_{sat}, γ_{sat} and θ_{sat}, for the 11 soil classes of the US Department of Agriculture (USDA) soil classification, based on measurements over large samples. Since our model specifies only one soil type everywhere, and because the determination of the above constants is not independent of the values of θ_{cap} and θ_{pwp}, we adopted the following procedure.

One of the fundamental properties of the soil, in its relation to the atmosphere, is the total-available water-holding capacity, or total availability (in m of water), representing the maximum amount of water that can potentially be extracted from the soil to fulfil evapotranspiration demands. This is the quantity that determines the slow-varying response of the soil. In fact, the soil acts as a low pass filter on the precipitation in such a way as to smooth the fluctuations of near-surface forcing (*Delworth and Manabe*, 1989). Soils with a larger total availability will be able to store water for longer periods and will have a longer time constant associated with them (*Milly and Dunne*, 1994). The soil cannot hold any amount of water in excess of field capacity for more than a couple of hours after a rainfall event, because of the strong non-linearity of equations (27): the practical upper-limit for the amount of water that can stay in the soil is then field capacity. For a fully vegetated grid-box, the lower limit for soil water content is the permanent wilting point, as can be seen from formula (17) for the soil water evaporative stress, and from the very low values of drainage at the bottom corresponding to $\gamma(\theta_{pwp})$. The volumetric available water-holding capacity, or availability (m^3m^{-3}), is given by

$$\theta_{ava} = \theta_{cap} - \theta_{pwp} \qquad (28)$$

Total availability is obtained by multiplying θ_{ava} by the total root depth.

A soil type representative for the whole world should be such as to represent the average response of the medium texture soils. Because our primary concern is availability, we looked in the literature for estimations of θ_{cap} and θ_{pwp}. A comprehensive review of measurements of the above two parameters may

be found in *Patterson* (1990). We start from Patterson's estimates of θ_{cap} and θ_{pwp} for the 11 USDA classes, and average the numbers corresponding to the medium texture soils (class 4, 5, 7, and 8, corresponding to silt loam, loam, silty clay loam and clay loam, respectively). The resulting numbers are θ_{cap}=0.323 m^3m^{-3} and θ_{pwp}=0.171 m^3m^{-3}. We get γ_{sat} and θ_{sat} by averaging the values of *Cosby et al* (1984) for the same classes. The numerical values are γ_{sat}=4.57 10^{-6} ms^{-1} and θ_{sat}=0.472 m^3m^{-3}. We now use the Clapp and Hornberger expression for the matric potential

$$\psi = \psi_{sat}\left(\frac{\theta}{\theta_{sat}}\right)^{-b} \tag{29}$$

with $\psi(\theta_{pwp})$=-153 m (-15 bar) and $\psi(\theta_{cap})$=-3.37 m (-0.33 bar) to find the remaining constants b and ψ_{sat}. The results are b=6.04 and ψ_{sat}=-0.338 m. The matric potential at permanent wilting point and field capacity are just large and small values respectively which are commonly used as a definition of wilting point and field capacity (see *Hillel*, 1980).

The above process ensures a soil that has an availability corresponding to the average value of the medium texture soils, and yields a quantitative definite hydraulic meaning to θ_{cap} and θ_{pwp}, compatible with the Clapp and Hornberger relations (See Table I for a summary of the soil constants). Note that, because the total root depth is 1 m (see next section), the above values give a total availability of 15.2 cm, very close to the value of 15 cm used in *Manabe* (1969), and by most of the bucket models since.

The soil properties as defined above also imply a maximum infiltration rate at the surface, defined by the maximum downward diffusion from a saturated surface. If the throughfall exceeds the maximum infiltration rate, the excess precipitation is put into runoff. However, in practice the maximum infiltration rate is so large that it is never reached. Runoff is therefore only produced when the soil becomes saturated.

2.4.3 *Discretization and the root profile*

We have chosen the same soil discretization for the thermal and water soil balance, for ease of interpretation of the results and simplicity of the code. However, most of the considerations given in section 2b, when discussing the impact of a particular choice of discretization on the thermal diffusion equation, are hardly relevant for the soil water budget. The main forcing for the soil water is the precipitation flux, which is a quasi-random time series, as opposed to the forcing of the thermal part, the harmonic time series of clear sky radiation, modulated by the presence of clouds. The relevant quantity for water, once the soil availability has been chosen (determined by the type of soil, see above section), is the total root depth. We have chosen a total root depth of $D_1+D_2+D_3$=1 m; visual inspection of the root depth maps of *Patterson* (1990), shows that this is an intermediate value, exceeded for some crops like corn, over North America and

Australia, and coniferous and deciduous forests of North America and Eurasia. Since the lowest model layer has no roots, it can act as a recharge layer, bringing water up to the root zone through diffusion during extensive dry spells.

Equations (21) and (22) are discretized in space in a similar way to the temperature equations. However, we found problems in time integrations with the "locally" implicit method explained in 2b: under certain forcing conditions, there was evidence of a bounded oscillation, that could be explained by a simple stability analysis of the numerical method. We therefore adopt a "global" semi-implicit scheme:

$$\rho_w \frac{\theta_i^{n+1} - \theta_i^n}{\Delta t} = -\frac{F^*_{i+1/2} - F^*_{i-1/2}}{D_i} + \rho_w S_{\theta,i} \tag{30}$$

$$F^*_{i+1/2} = -\rho_w [\lambda_{i+1/2} \frac{\theta^*_{i+1} - \theta^*_i}{0.5(D_i + D_{i+1})} - \gamma_{i+1/2}] \qquad i=1,2,3 \tag{31}$$

where $F_{i+1/2}$ is the flux of water at the interface between layer i and $i+1$, $\rho_w S_{\theta,i}$ is the root extraction at layer i, and

$$\theta^*_i = \alpha_I \theta_i^{n+1} + (1-\alpha_I)\theta_i^n \tag{32}$$

α_I, is the implicit coefficient, α_I=1.5. For improved accuracy, the hydraulic diffusivity and conductivity are taken as (see *Mahrt and Pan*, 1984)

$$\begin{aligned} \lambda_{i+1/2} &= \lambda[\max(\theta^n_i, \theta^n_{i+1})] \\ \gamma_{i+1/2} &= \gamma[\max(\theta^n_i, \theta^n_{i+1})] \end{aligned} \tag{33}$$

The boundary conditions are given by

$$\begin{aligned} F_{41/2} &= \rho_w \gamma_4 \\ F_{1/2} &= T - Y_s + E_{1/2} \end{aligned} \tag{34}$$

The difference between throughfall T and surface runoff Y_s ($kgm^{-2}s^{-1}$) is the soil infiltration at the surface. The evaporation at the top of the soil layer, $E_{1/2}$, is computed as

$$E_{1/2} = (E - E_l^*)\frac{(1-C_v)E_g}{C_v E_v} \tag{35}$$

Equation (35), together with the treatment of interception reservoir evaporation and the repartition of the dry vegetated evaporation in root extraction at the different layers, conserves the total amount of water evaporated to the atmosphere. Root extraction is computed as

$$\rho_w S_{\theta,i} = (1-C_l)C_v \frac{E_v}{D_i} \frac{R_i\theta_i}{\sum_k R_k\theta_k} \qquad i=1,2,3$$

$$\rho_w S_{\theta,4} = 0 \tag{36}$$

In case of dew deposition, $S_{\theta,i}$=0. The integration scheme detailed in equations (30-32) is flux conservative. It can be shown to be stable and to have a non-oscillatory behaviour.

Similarly to the analysis of time scales of the different layers for diffusion of heat in section 2b we can analyze the time scales for diffusion and drainage of soil moisture. Because the soil diffusivity and conductivity depend strongly on soil moisture, we compute the time constants at percentages of availability between field capacity and permanent wilting point. It can be seen from Table 3 that the time scales are short for moist soil and become very long for dry soil. The asterisks in the table indicate that, for dry soil moisture values, diffusion and drainage do not play an important part in the evolution of soil moisture at the deeper layers. In particular, they show that the lowest model layer acts as a slow recharge layer to the layers above.

	0 %	33 %	67 %	100 %
1 upwards	-	-	-	-
1 downwards	19.7	2.5	0.5	0.1
1 drainage	**	**	188.5	17.7
2 upwards	59.0	7.6	1.4	0.4
2 downwards	195.9	25.1	4.7	1.2
2 drainage	**	**	565.6	53.2
3 upwards	671.5	86.2	16.1	4.2
3 downwards	**	241.9	45.2	11.7
3 drainage	**	**	**	182.3
4 upwards	**	635.0	118.6	30.7
4 downwards	-	-	-	-
4 drainage	**	**	**	478.6

Table 3 Moisture time scale (in days) associated with each layer, dependent on soil moisture (percent of maximum availability). See text for an explanation of the different quantities. ** indicates values larger than 1000 days (see text for further discussion).

3. POINT VALIDATION

In this section we use field data to test the parametrization described above (identified with model cycle 48). We also compare with the old parametrization (model cycle 47), which is described in the Appendix and further documented by *Blondin* (1991). The two versions of the land surface parametrization and the surface

layer part of the boundary layer scheme (cy47 and cy48) are driven, in stand-alone mode, with observational time series of wind, temperature, specific humidity, precipitation and downward radiation (solar and thermal) as forcing boundary conditions. The model variables at the lowest model level are replaced by the observational time series and the height of the lowest model level is replaced by observation height (above displacement height). In this way only the surface layer part of the boundary layer scheme and the entire land surface code are used and tested. The advantage is that we study the performance of the land surface code without complicated interactions with other parts of the model. The land surface scheme could for instance have impact on precipitation, cloud cover and radiation, but we exclude such interactions because precipitation and atmospheric radiation are prescribed from observations. Therefore we can concentrate on the land surface scheme, without considering deficiencies from other parts of the model. This validation strategy is also proposed in phase II of the Project for Intercomparison of Land surface Parametrization Schemes (PILPS, see *Henderson-Sellers et al*, 1993).

The aim of the current study is not to optimize the parametrization for a particular location, but rather to check the performance of the scheme in different climatological regimes, with emphasis on the seasonal time scale. We use three different datasets: FIFE 1987 data from Kansas USA (*Sellers et al*, 1988), data from Cabauw in The Netherlands (*Beljaars and Viterbo*, 1994) and ARME data from central Amazonia (*Shuttleworth et al*, 1984a). The model parameters are not adjusted to these experimental sites but have the values that are used in the global model for these locations. Note that in this we differ from the PILPS methodology: In PILPS, all models are given a common set of parameters characteristic of the locations, allowing a more straightforward comparison between the different models (*Pitman at al*, 1993). Geographically constant soil and vegetation types are part of the features of both model cycles 47 and 48, and therefore those global values are chosen for the validation presented in this section. The parameters that depend on geographical location in the ECMWF model are specified in Table IV for the three sites and the two model versions. Initial profiles in the soil are set to a climatological value for temperature and to model field capacity, θ_{cap}, for soil moisture. For all locations, the results are not very sensitive to the initial conditions because the initial conditions are sufficiently wet that the soil has a short response time. Sensitivity to model parameters, to reflect more closely the different experiment locations, instead of global model values for these locations is not studied here.

		albedo	z_{0m} (m)	z_{0h} (m)	veg cover	obs hei (m)
FIFE	cy47	0.17	0.3	0.3	0.85	-
39°03'N	cy48	0.17	0.3	0.03	0.85	-
96°32'W	obs	0.17-0.21	0.19	0.01	-	2
Cabauw	cy47	0.17	0.4	0.4	0.87	-
51°58'N	cy48	0.17	0.4	0.04	0.87	-
4°56'E	obs	0.23	0.1	0.0001	-	20
ARME	cy47	0.13	2.5	2.5	0.94	-
3°S	cy48	0.13	2.5	0.25	0.94	-
60°W	obs	0.12	1.7	-	-	13

Table 4 Model parameters for the different experimental sites

3.1 **FIFE**

3.1.1 *FIFE location and data*

The FIFE experimental domain consists of 15x15 km tallgrass prairie on a rather complex undulating topography. The growing season is from May to October, with the leaf area index having a maximum of about 3 toward the end of June, which gradually decreases with plant senescence in September and October (*Kim and Verma*, 1990). Soil is predominantly Benfield-Florence complex and Clime-Sogn complex, with estimated averaged soil properties of 0.47, 0.39 and 0.17 m^3/m^3 for saturation value, field capacity and wilting point respectively (*Famiglietti et al*, 1992). The observed albedo is between 0.18 and 0.21 in October and about 0.02 lower in August (*Betts et al*, 1993); the roughness lengths for momentum and heat are estimated by *Betts and Beljaars* (1993) to be 0.19 m and 0.01 m respectively.

The FIFE dataset consists of nearly continuous observations of surface parameters from the Portable Automated Mesonet stations (PAM) covering the period from 1 May 1987 to 16 October 1987 and four Intensive Field Campaigns (IFC's) with surface flux observations (from 26 May to 7 June, from 25 June to 11 July, from 6 to 21 August and from 5 to 16 October). The PAM data (30-minute averages at 10 stations) consists of wind at 5.4 m, temperature and humidity at 2m, together with radiometric measure of the ground surface temperature, downward short wave radiation, net radiation, downward long wave radiation and rainfall. During the IFC's, fluxes of sensible and latent heat and ground heat flux were measured at about 13 stations with Bowen and eddy correlation methods. The PAM data have been quality controlled, edited and averaged by *Betts and Ball* (1992) (see also *Betts et al*, 1993, for details) resulting in a single time series, representing the average over an area of 15x15 km. The wind at 5.4 m has been interpolated to the 2 m level with the routines described by *Beljaars and Holtslag* (1990) using Monin Obukhov similarity and surface fluxes. Also the flux data has been averaged over all the available stations

during the IFC's. The resulting averages are believed to be representative for the 15x15 km square. All the observations are available as a time series of half hour averages.

The PAM dataset is virtually continuous and can be used as atmospheric boundary conditions for the land surface module in a single column mode. Verification can be done by comparing with surface fluxes during the IFC's. It is more interesting, however, to verify the water budgets over the entire time interval from May to October. For that purpose we use the heat fluxes from continuous temperature profile observations of two stations (stations 2 and 28 from 27 May to 16 October; see *Smith et al*, 1992). The latent heat flux has been inferred by *Smith et al* (1992) as a residual from the surface energy balance. These two stations have Bowen observations during the IFC's and profile observations in between IFC's. *Smith et al* (1992) compare the two methods and find good agreement. To see whether these flux observations are representative for the entire FIFE area, we compare them with the averages of the IFC's. The following parameters are compared: (i) diurnal averages of net radiation, sensible and latent heat flux in Fig 2, and (ii) midday averages (between 16 and 20 h UTC, 4 hours centred around local noon) of these quantities in Fig 3. The agreement between the averages of the IFC's and the continuous time series of the two Bowen stations is very good. Also the time series from stations 2 and 28 are remarkably similar although small differences can be observed. When integrated over the entire measuring period, station 38 has 6% less net radiation, 8% less latent heat flux and 8% less sensible heat flux than station 2. The differences in latent heat flux are largest between day 200 and day 215 and between day 248 and day 288, when the vegetation is stressed. The difference between the two stations is probably related to their location: station 2 is in a valley whereas station 38 is at the top of a ridge. As we will see later, the differences between stations are small compared to the model deficiencies we want to address. So we conclude that the two time series of continuous flux observations are sufficiently representative for the FIFE area to study model problems related to the seasonal time scale.

The evolution of soil moisture was also monitored during the FIFE experiment and is shown in Fig 4. Gravimetric soil moisture measurements were taken for the subsurface layers from 0-5 cm and 5-10 cm deep at about 10 days intervals together with volumetric soil moisture profiles from neutron probe soundings (*Strubel et al*, 1991). The gravimetric observations had a higher frequency during the IFC's. To allow comparison with model results, the gravimetric data has been converted to volumetric units using a "dry soil density" of 1100 kg/m^3. However, large uncertainties in soil density have been reported; *Wang* (1992) mentions a range of 700 to 1400 kg/m^3. The neutron probe observations were taken at depths from 30 cm to 200 cm. The 30 cm level has been discarded, because of evident biases (probably because of surface effects on the neutron scattering). Averages have been computed over all the observations available in the FIFE area. The number of points used for the averaging is about 140 for the gravimetric observations and decreases gradually with depth for the neutron probe data from about 70 at a depth of 40 cm to about 10

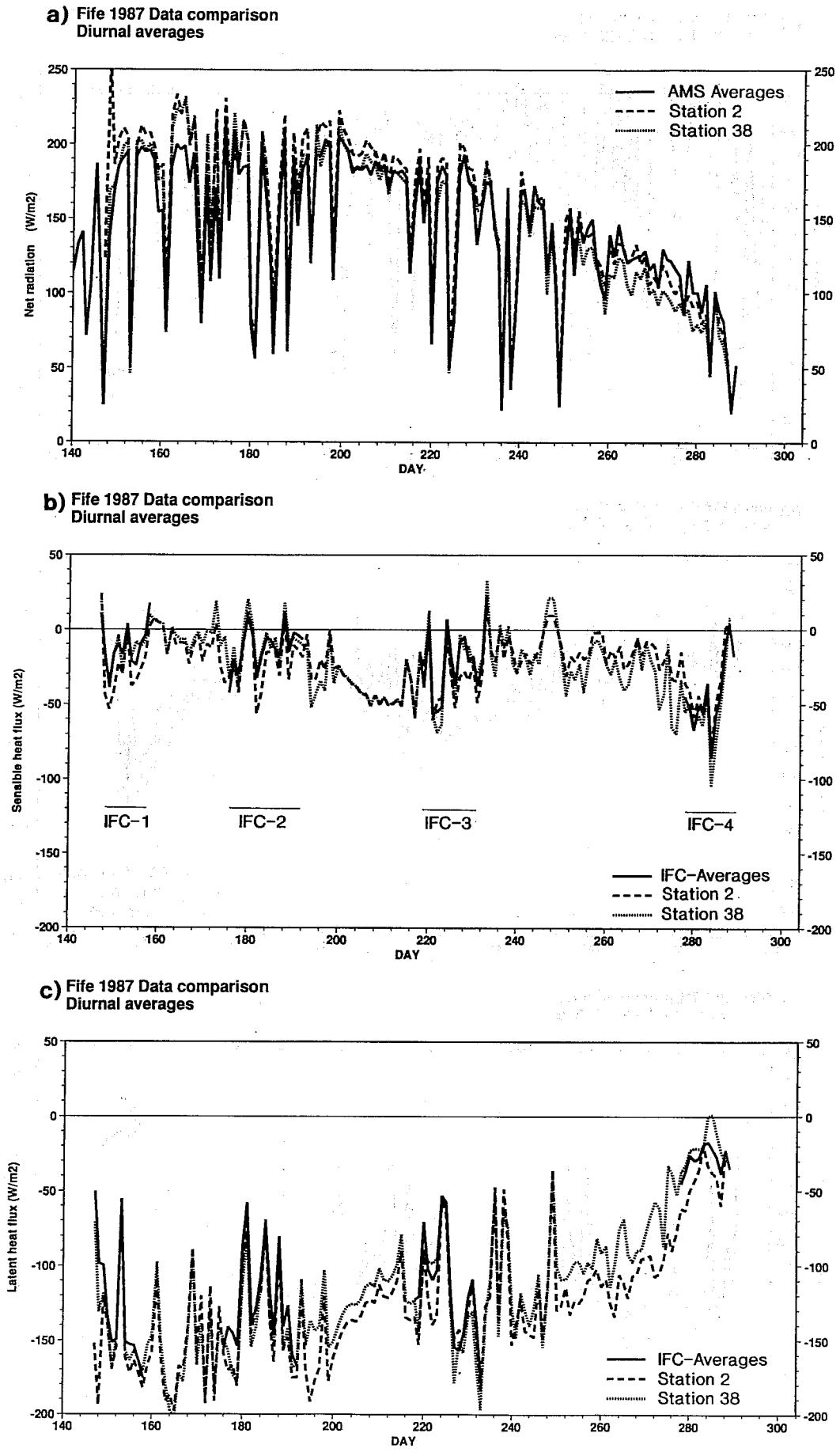

Fig 2 Diurnal averages of surface energy budget. Fig a compares net radiation from the AMS stations (averaged over all stations) with net radiation from stations 2 and 38. Figs b and c compare sensible and latent heat fluxes respectively (averaged over all stations during the IFC's) with those from stations 2 and 38.

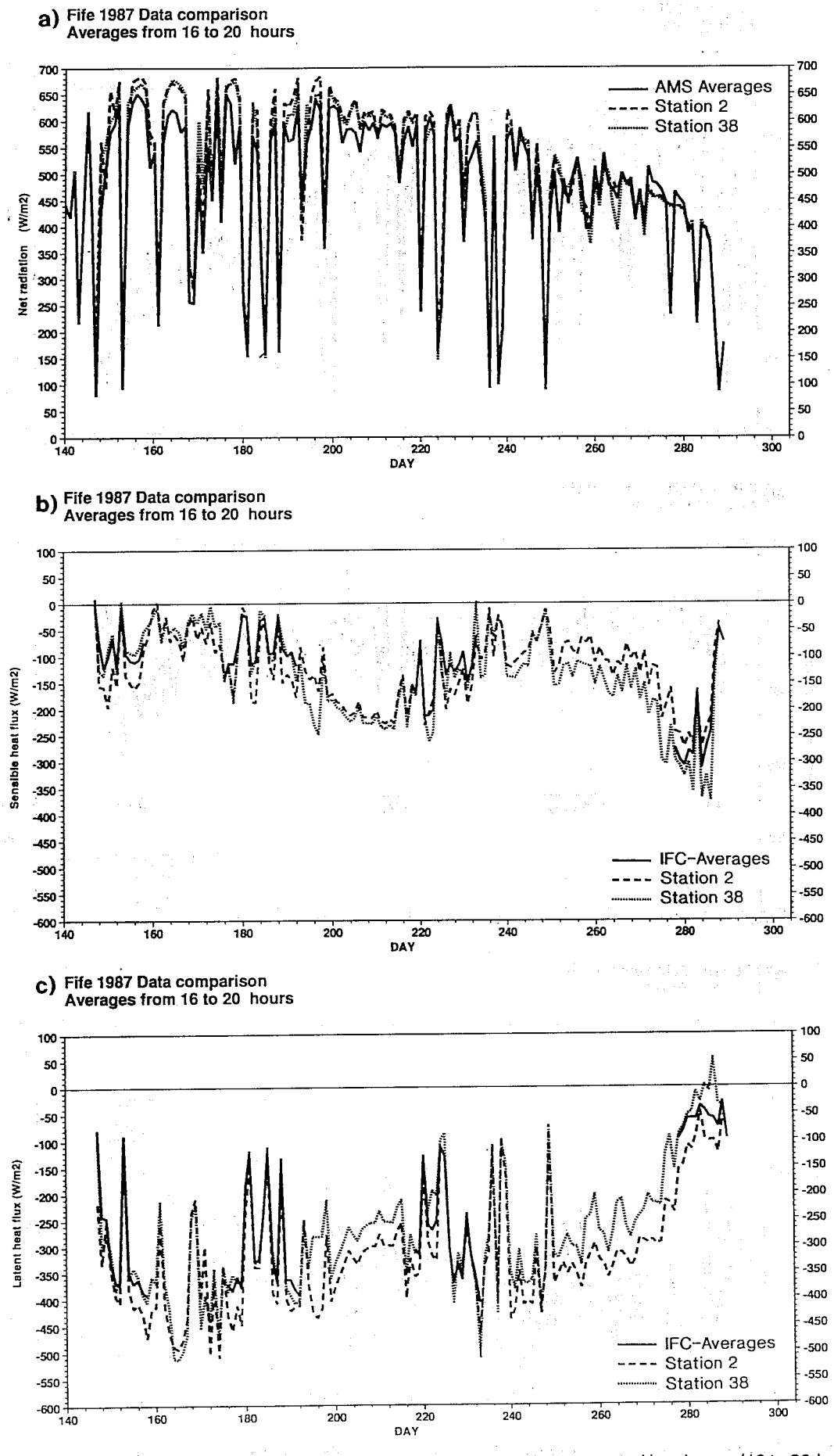

Fig 3 As Fig 2 but for the midday averages. Averages are taken over 4 hours around local noon (16 to 20 hours UTC).

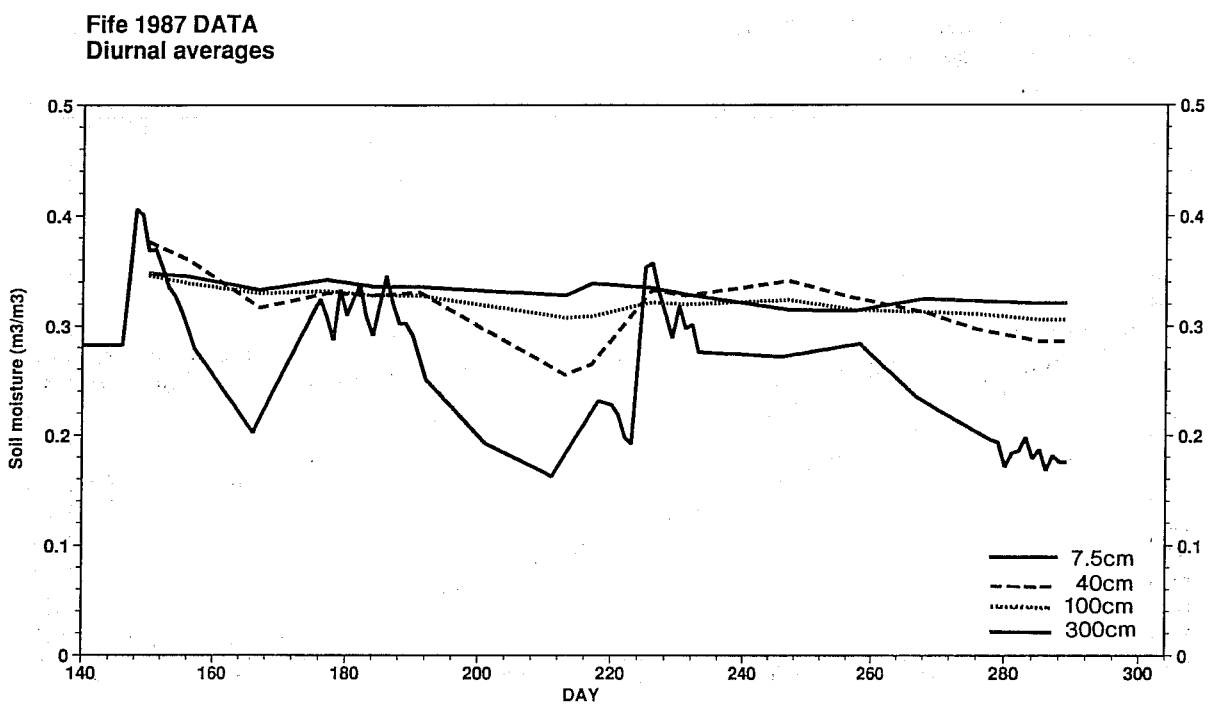

Fig 4 Evolution of observed soil moisture at depths of 7.5 cm (gravimetric observations converted to volumetric units), 40 cm, 100 cm and 200 cm (neutron probe data in volumetric units).

at a depth of 200 cm. The neutron probe profiles were not always measured on the same day for the entire area. When profiles were measured one or two days apart they are still averaged to a single profile, which implies that the interpretation of these profiles is only useful on longer time scales.

The observed seasonal evolution of soil moisture at different levels, as shown in Fig 4, clearly reflects the effects of continuous drying through evapotranspiration and the moistening from precipitation events. Thisis even more clear from the time integrated precipitation plus evaporation in comparison with the change in soil water content vertically integrated over a depth of 2 m (Fig 5; note that the model convention is used with positive values for downward fluxes). Although the curves are similar in shape, there is also a considerable mismatch: the drying of the soil is less rapid than expected from the time integrated P+E. Over the time period from day 147 to 289, the difference is nearly 100 mm. The reason for this discrepancy is not very clear. It cannot be explained by runoff because any runoff would make the difference even larger. However, the uncertainty in the different terms of the budget is quite large. The budget comparison of Fig 5 suggests that precipitation is a less likely candidate for the mismatch, because the error is mainly during soil drying rather than during the moistening events. The difference in slope between soil drying and (P+E) is about 20% for the drying period from day 257 to 285. It is also possible that some of the soil moisture for evapotranspiration comes from below 2 m.

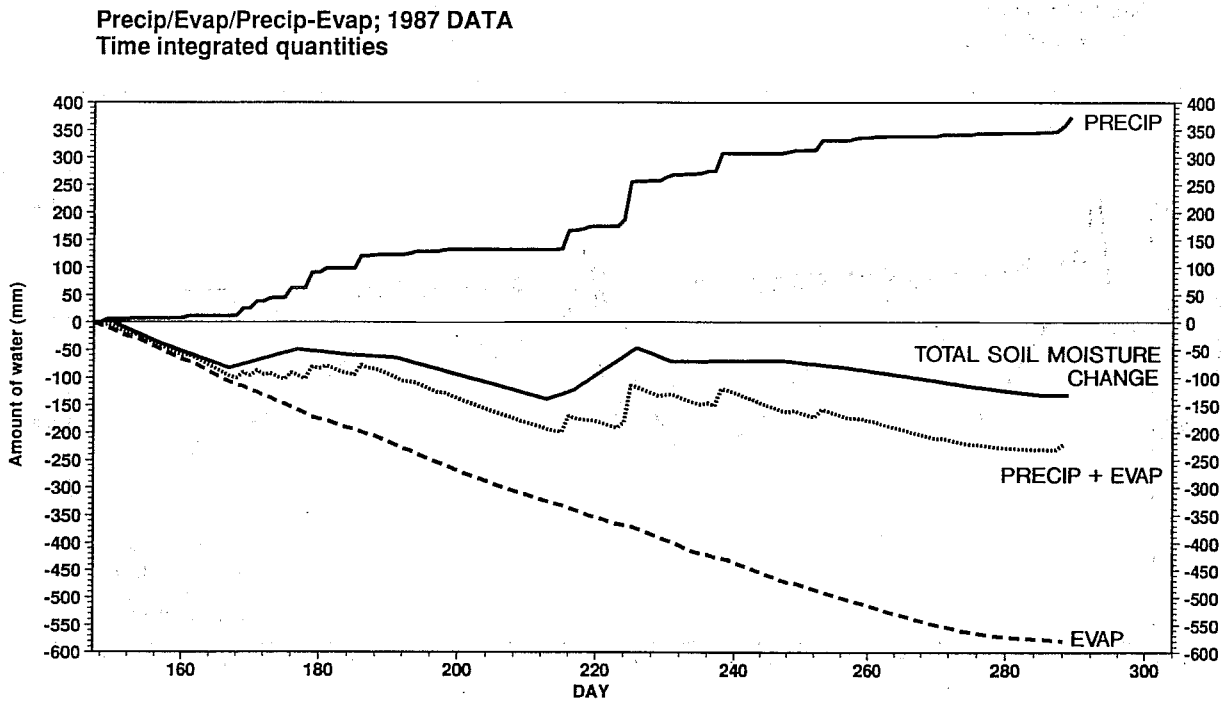

Fig 5 Accumulated precipitation (P), evaporation (E) and P+E in comparison with the change of soil moisture integrated over a depth of 2 m. These are observations averaged over all data available in the FIFE area.

3.1.2 *One column simulations for FIFE*

The simulations with FIFE data start from 1 May 1987 (day 121) with soil moisture initialized at field capacity and soil temperature initialized at the ECMWF climatological value for May. Here, as for the next data sets, we will concentrate our discussion on aspects related to soil hydrology. Direct benefits of the use of skin temperature in cycle 48, in terms of a smaller ground heat flux, are documented for FIFE in *Beljaars and Betts* (1993) and can also be seen in Figs 17-19 for the GCM simulations. The comparison with data is from 27 May (day 147) to 16 October (day 289) and is shown in the Figs 6-10. The diurnal averages of latent heat flux produced with cycle 48 agree much better with observations than the fluxes from cycle 47 (Fig 6). The evaporation with cycle 47 is influenced quite strongly by its climatological lower boundary condition, whereas cycle 48 can sustain evaporation for quite some time after precipitation events. This is also illustrated by the midday evaporative fraction (Fig 7) and the accumulated moisture budget (Fig 8). It should be noted that the agreement between model cycle 48 and data is much better during the IFC's than between the IFC's (compare Fig 7 and Fig 2); this may be an indication that the data is less reliable outside the IFC's, where the profile method has been used instead of the Bowen method to derive sensible and latent heat fluxes.

The difference between model cycle 47 and 48 is most evident from the soil moisture evolution (Fig 9) and from the soil moisture profiles (Fig 10). Cycle 47 has an unrealistic response to precipitation events, and evaporation is influenced rather strongly by the climate layer. With the constant value of the diffusion coefficient, the diffusion of moisture between the layer 3 (boundary condition) and layer 2 is 2.1 mm/day

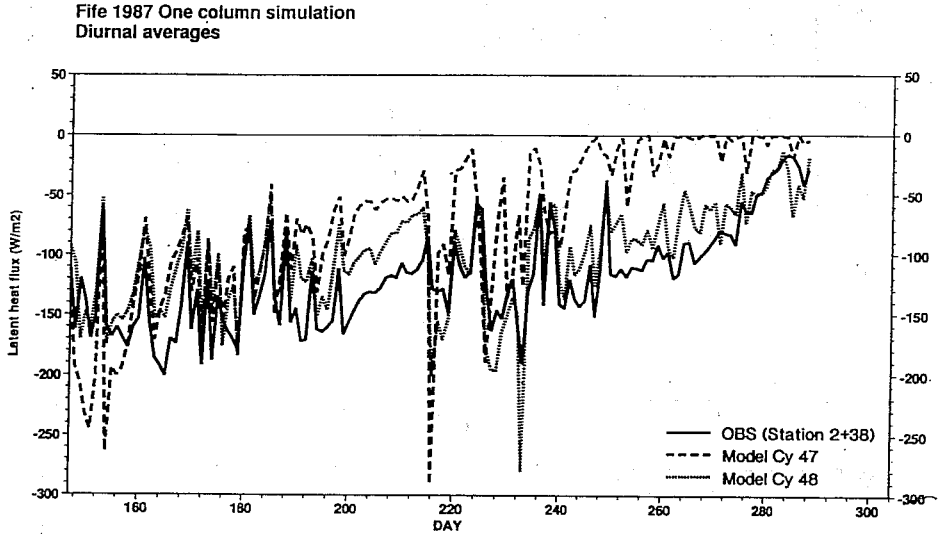

Fig 6 Diurnal averages of latent heat flux for FIFE, simulated with model cycles 47 and 48 and observed. The observations are the average of station 2 and station 38 from *Smith et al* (1992).

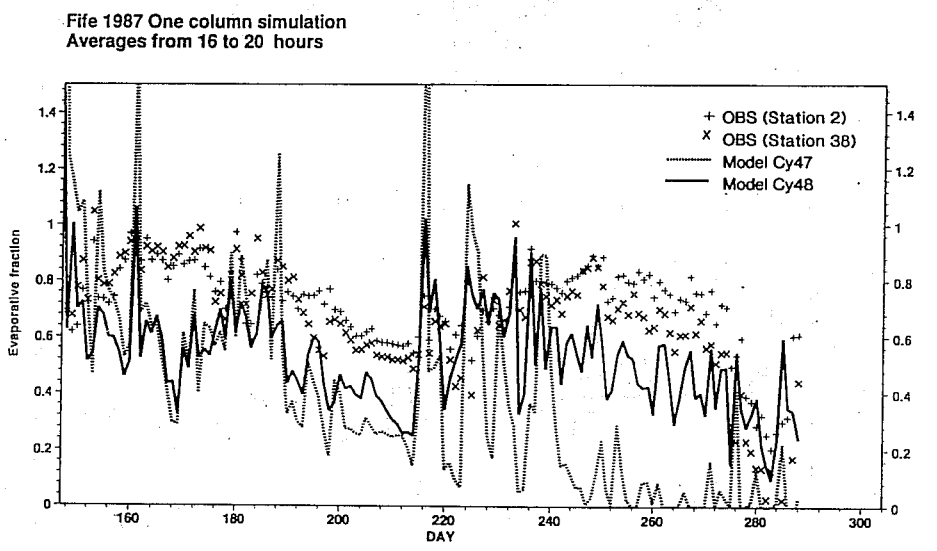

Fig 7 Midday averages (averaged over 4 hours around local noon) of evaporative fraction with model cycles 47, 48 and FIFE observations.

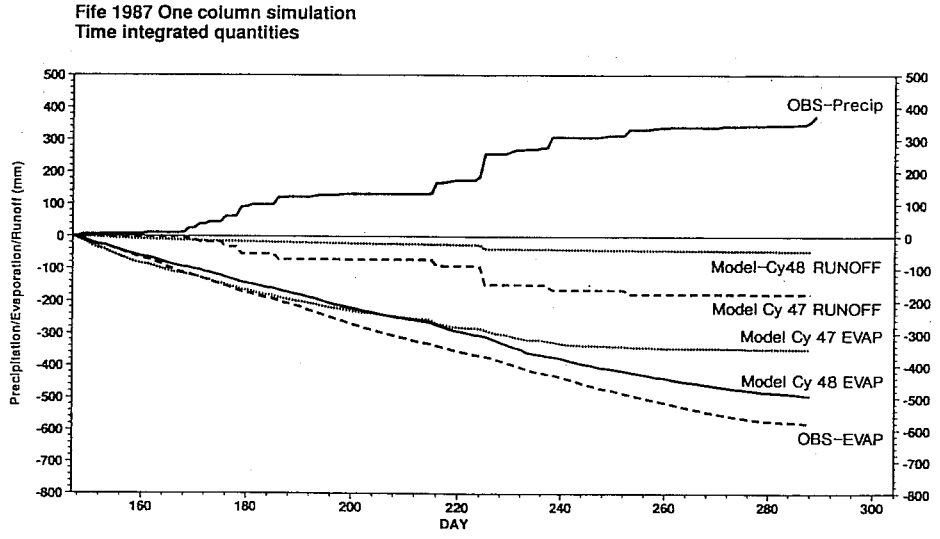

Fig 8 Accumulated moisture budget at the surface for FIFE.

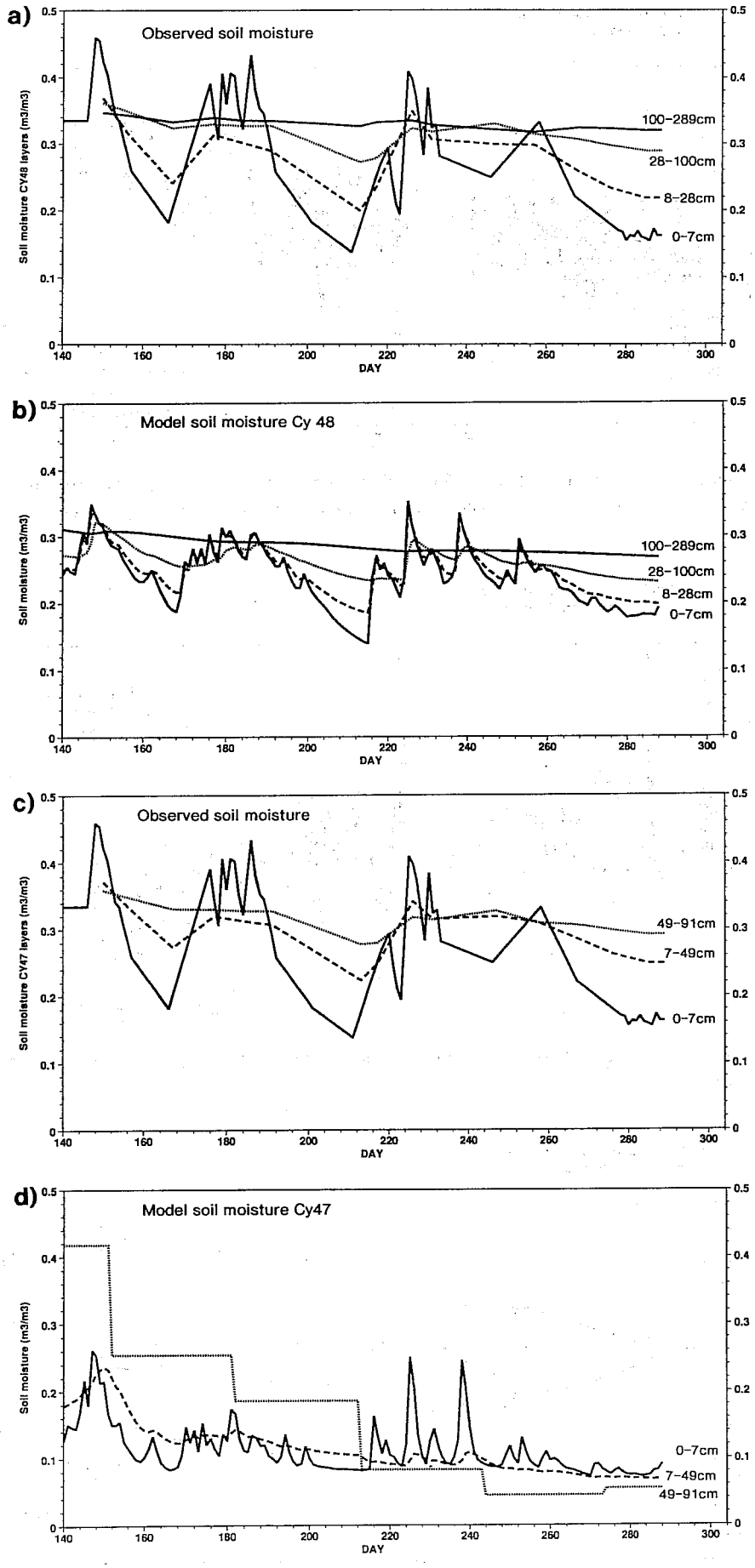

Fig 9 Seasonal evolution of soil moisture for FIFE with model cycle 47 (a), cycle 48 (c) and observed (b,d). The observations have been vertically integrated to mimic the model layers of cycle 47 (b) and cycle 48 (d). For model level 4 in cycle 48 the 200 cm observation has been extrapolated to a depth of 289 cm.

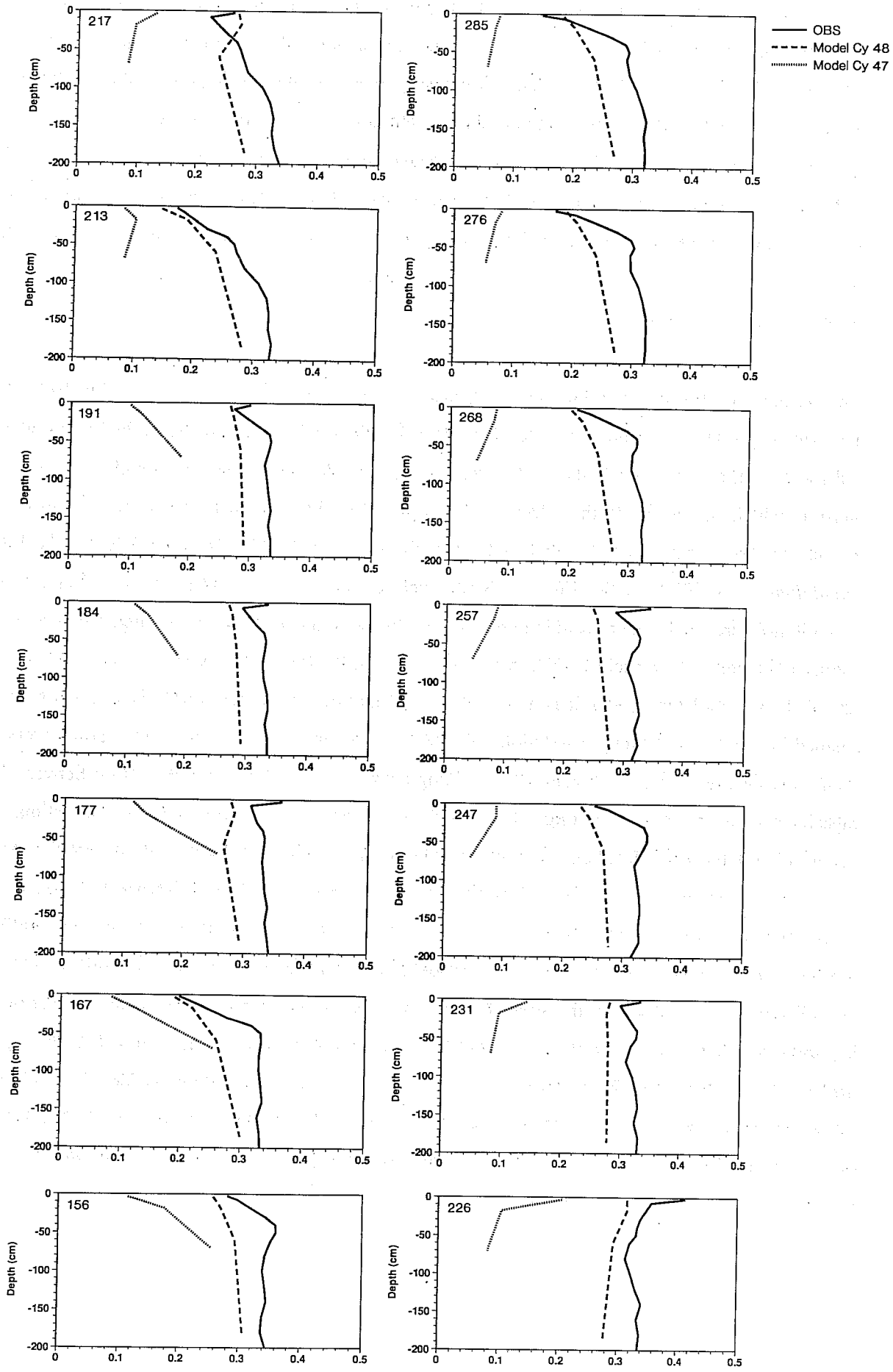

Fig 10 Soil moisture profiles for FIFE in comparison with profiles, simulated with model cycles 47 and 48.

for a volumetric soil moisture difference of 0.1 m^3/m^3, which results in considerable amounts of influx for May and June, but leads to rapid loss of water and subsequent reduction of evaporation after June. The runoff in cycle 47 is also rather unrealistic; it is nearly always a constant fraction of the precipitation even when the soil is rather dry. This is mainly due to saturation runoff at the surface, because the downward transfer of moisture is slow. Model cycle 48 behaves quite differently: because the moisture diffusion coefficients depend on soil moisture, the downward transport is very efficient after precipitation. Therefore the deeper layers can be filled easily without loosing all the precipitation through saturation runoff. Because the deeper layers are also filled by precipitation, the evaporation can be maintained for a much longer period of time than with cycle 47.

The soil moisture profiles with both model cycles and observed profiles are shown in Fig 10 for the days that neutron probe profiles are available. It is clear that the profiles with model cycle 48 look much more realistic than those with cycle 47. However, the new model has a systematic shift in volumetric soil moisture which can be due to the selection of soil properties in the model. The deep soil has a tendency to relax towards field capacity, which is 0.32 in the model and which is about 0.39 for the FIFE area (*Famiglietti et al*, 1992). This difference is relatively unimportant as far as the evaporation is concerned. The soil moisture can be interpreted in terms of availability (as a percentage in the range between permanent wilting point and field capacity) which makes the value of the field capacity irrelevant. However, the total size of the soil moisture reservoir is much more important because it determines how much water can be retained for evaporation after precipitation and determines an important time constant in atmospheric models (*Milly and Dunne*, 1994). The volumetric holding capacity of the soil is the difference between the field capacity and the permanent wilting point, which is .15 m^3m^{-3} for model cycle 48 and estimated to be .22 m^3m^{-3} for the FIFE location. The lower value in the model may be the reason that the model still underestimates evaporation at the end of the growing season. Another difference between model and observations concerns the near surface variability in soil moisture. The observed soil moisture profiles show much larger variability than the model. The model simulations have rather smooth profiles. The detail of the soil moisture weighting in the stress function and the vertical distribution of root extraction play an important role here. The root extraction profile, as chosen in equation (18), ensures that the top layer is depleted faster than layer 2 and so on. The evolution of the soil moisture profile of the observations following precipitation events (compare day 213 with day 191 and day 268 with 267 in Fig 10) confirm that, although they indicate an even stronger variation with height. The observations suggest a gradual depletion of soil water from top to bottom.

3.2 Cabauw

3.2.1 *Cabauw location and data*

The Cabauw data used in this study have been collected at the 200 m meteorological mast in Cabauw in the Netherlands. This site is located in flat terrain consisting mainly of grassland interrupted by narrow ditches. Up to a distance of 200 m from the mast, there are no obstacles or perturbations of any importance; further on some scattered trees and houses are found for most wind directions (see *Driedonks et al*, 1978, for a more detailed description). The soil consists of a 1 m deep layer of clay on top of a 10 m deep layer of peat saturated with water. The bottom part of the clay layer is always in an artificially maintained water table. *Holtslag and Van Ulden* (1983) suggest an albedo of 0.23 for this site and roughness lengths of momentum and heat are estimated to be 0.1 and 0.0001 respectively (*Beljaars and Holtslag*, 1991).

In this paper we use the observations of wind, temperature and specific humidity at a height of 20 m as a boundary condition for the one column soil model. All quantities are averages over 30 minute intervals for the year 1987. For verification, fluxes of sensible and latent heat have been derived from net radiation, ground heat flux and profiles of wind temperature and moisture. When data are missing because of instrument failure or data transmission problems, the dataset is filled in with help of observations from SYNOP station De Bilt 30 km away. A simple procedure (*Beljaars and Holstlag*, 1990) was used to simulate the surface fluxes, to interpolate to the 20 m level and to correct for differences in terrain roughness. Although the methods used in the procedure have been extensively verified against data and are in fact tuned to this particular site (*Holtslag and Van Ulden*, 1983), the interpolated data cannot be considered to be real verification material. However, the amount of filled in data is small (about 10-20% dependent on parameter) and the procedure enables us to look at integrated budgets. The dataset has been prepared for the entire year of 1987 (see *Beljaars and Viterbo*, 1994 for more details).

3.2.2 *One column simulations for Cabauw*

The simulations with Cabauw data are started from 1 January 1987 with soil moisture initialized at field capacity and soil temperature at the climatological value of January. The comparison of simulations (cycle 47 and 48) with data are shown in Figs 11-13. The impact of the model change is quite different from the impact on the FIFE simulation. For FIFE the new model increases the evaporation, mainly by reducing the runoff. For Cabauw the new model reduces evaporation and increases runoff. The precipitation regime at Cabauw is very different from FIFE. At Cabauw precipitation comes in small amounts throughout the year, which implies that evaporation is seldom supply limited. Evaporation is reduced with cycle 48 compared to 47, because both the minimum stomatal resistance and the aerodynamic resistance have been increased by selecting a smaller roughness length for heat and moisture. The latter is of particular importance for winter situations with water on the vegetation (see *Beljaars and Viterbo*, 1994 for a more detailed analysis).

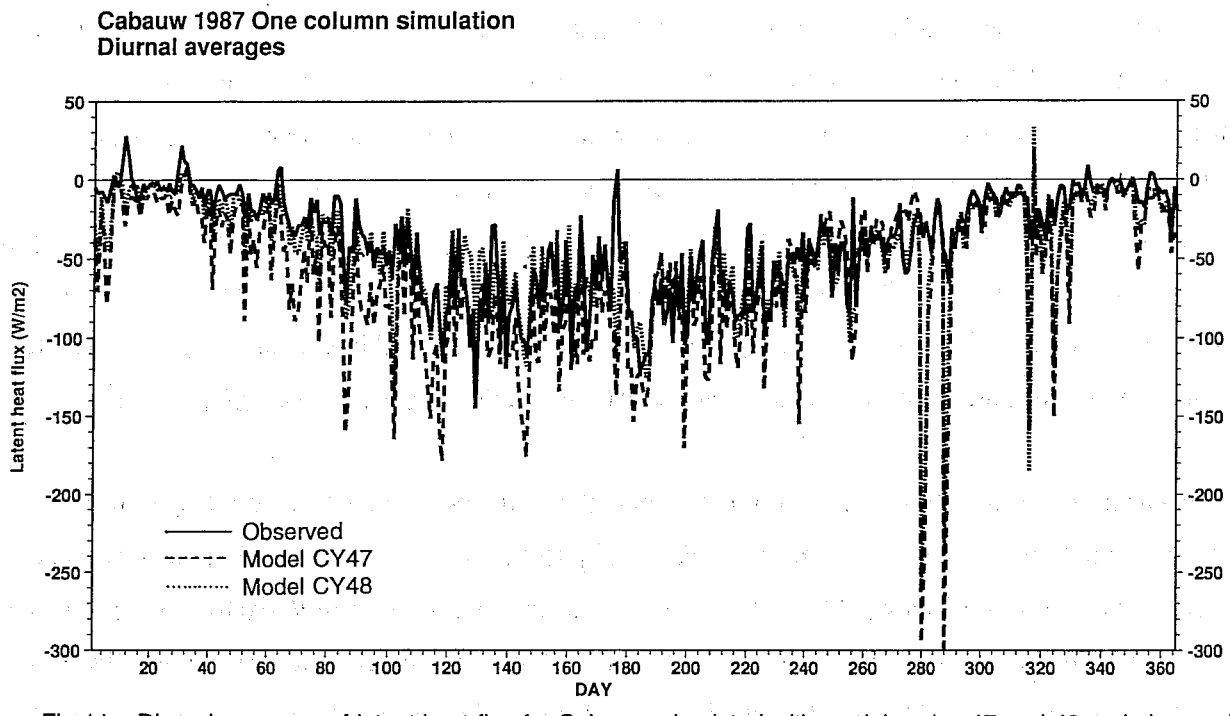

Fig 11 Diurnal averages of latent heat flux for Cabauw, simulated with model cycles 47 and 48 and observed.

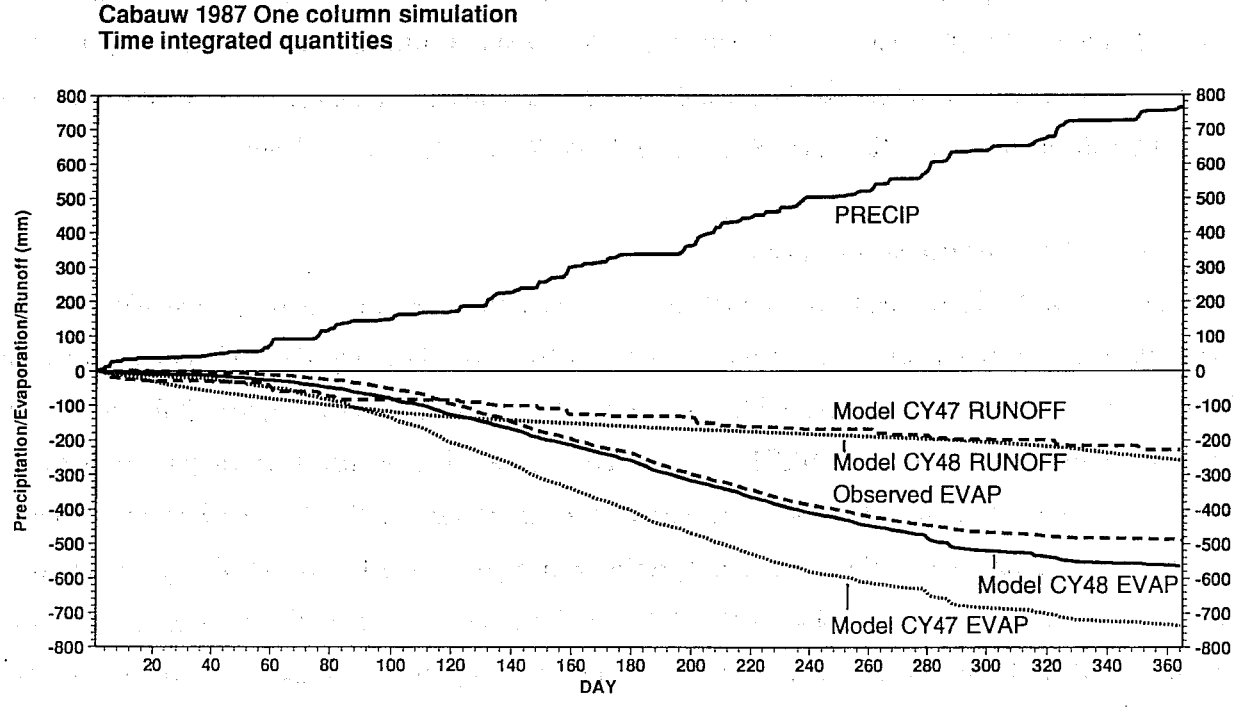

Fig 12 Accumulated moisture budget at the surface for Cabauw.

a) Cabauw 1987 One column simulation
Diurnal averages

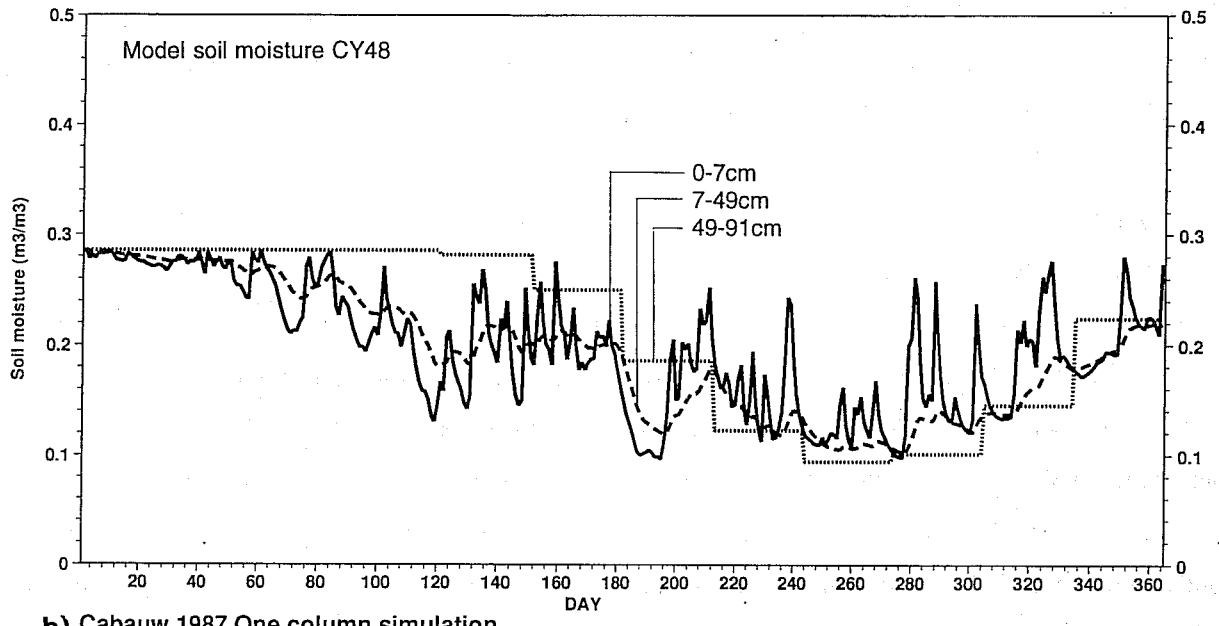

b) Cabauw 1987 One column simulation
Diurnal averages

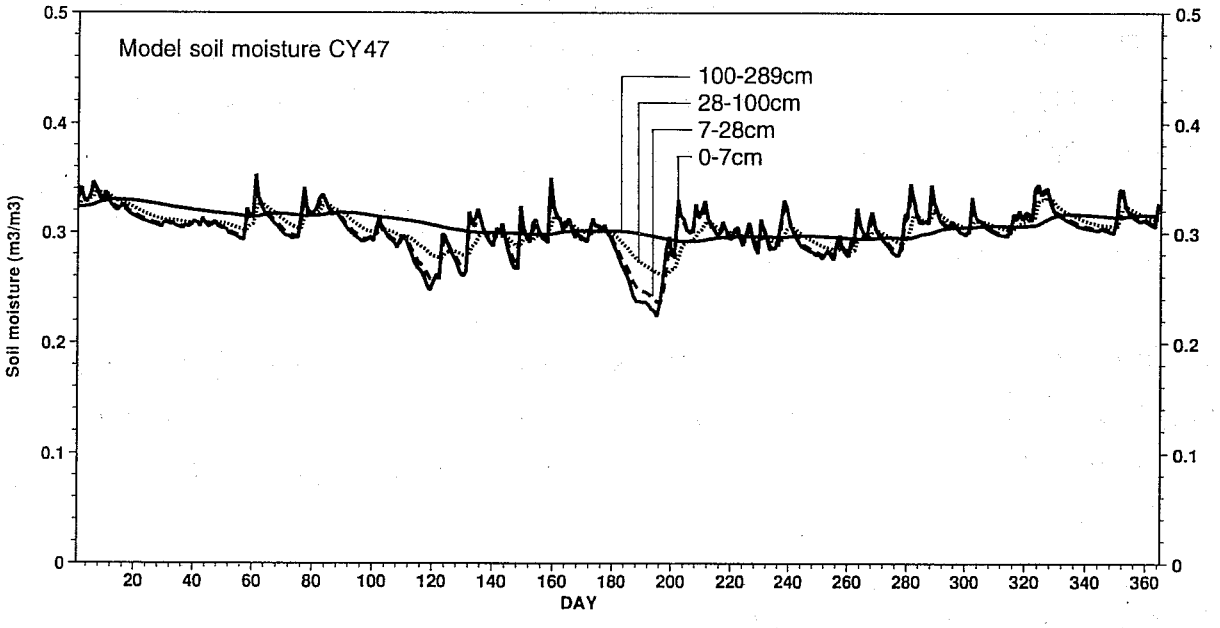

Fig 13 Seasonal evolution of soil moisture for Cabauw with model cycle 47 (a), cycle 48 (b).

The effect of the aerodynamic resistance is also reflected in the large extremes with cycle 47 in the diurnal averages of latent heat flux (Fig 11). These extremes are mainly during days with strong wind.

The seasonal evolution of soil moisture is again more realistic with cycle 48 than with cycle 47. The largest amplitude in soil moisture variations is at the surface with cycle 48, whereas cycle 47 has a large seasonal amplitude driven from the deep soil boundary condition (Fig 13).

3.3 **ARME**

3.3.1 *ARME location and data*

The ARME site was in terra firma forest located in the Reserva Florestal Ducke, 25 km from Manaus, Amazonas Brazil and was selected as representative of natural vegetation and regional topography (see *Shuttleworth et al*, 1984a; *Shuttleworth*, 1988). Routine meteorological observations were taken from 1 September 1983 to 30 September 1985 at a height of 45 m, approximately 10 m above the forest canopy. The hourly observations of wind, temperature, humidity, rainfall and radiation are used as a forcing boundary condition to the one column model. Rainfall interception is determined as the difference between precipitation and throughfall. *Lloyd and Marques* (1988) studied the sampling errors and the reliability of the interception estimates and conclude that they can only be used when integrated over an extended period of time. Fluxes of sensible and latent heat were measured during September 1983, July and August 1984 and March to August 1985, using eddy correlation techniques above the forest on the same tower as the automatic weather station (*Shuttleworth et al*, 1984a). The long term imbalance between net radiation and the sum of sensible and latent heat flux is about 9%, which is interpreted as a "flux loss" in the eddy correlation instrument (*Shuttleworth et al*, 1984a).

Rooting in the soil is dense down to 15 cm, but it is known that the forest can routinely access soil water to a depth of 1 m and to at least 2 m during prolonged dry periods (*Shuttleworth et al*, 1984a). The observed albedo is 0.12 and the roughness length for momentum is estimated to be 1.7 (*Shuttleworth et al*, 1984b; *Shuttleworth*, 1988).

3.3.2 *One column simulations for ARME*

The simulated latent heat flux and the accumulated surface moisture budget are shown in Figs 14 and 15 for model cycle 47 and 48. The day numbers are counted from 1 January 1983. The main difference between the two models is the reduced annual cycle with model cycle 48. The rainfall exhibits a marked seasonal dependence with a mean monthly maximum of about 350 mm in March and a minimum of around 100 mm in August. This is reflected in the deep soil moisture by *Mintz and Serafini* (1992) which forces the annual cycle in evaporation with model cycle 47. The annual variation is even more obvious in the evaporative fraction at local noon (see Fig 16). The data does not show any sign of an annual cycle

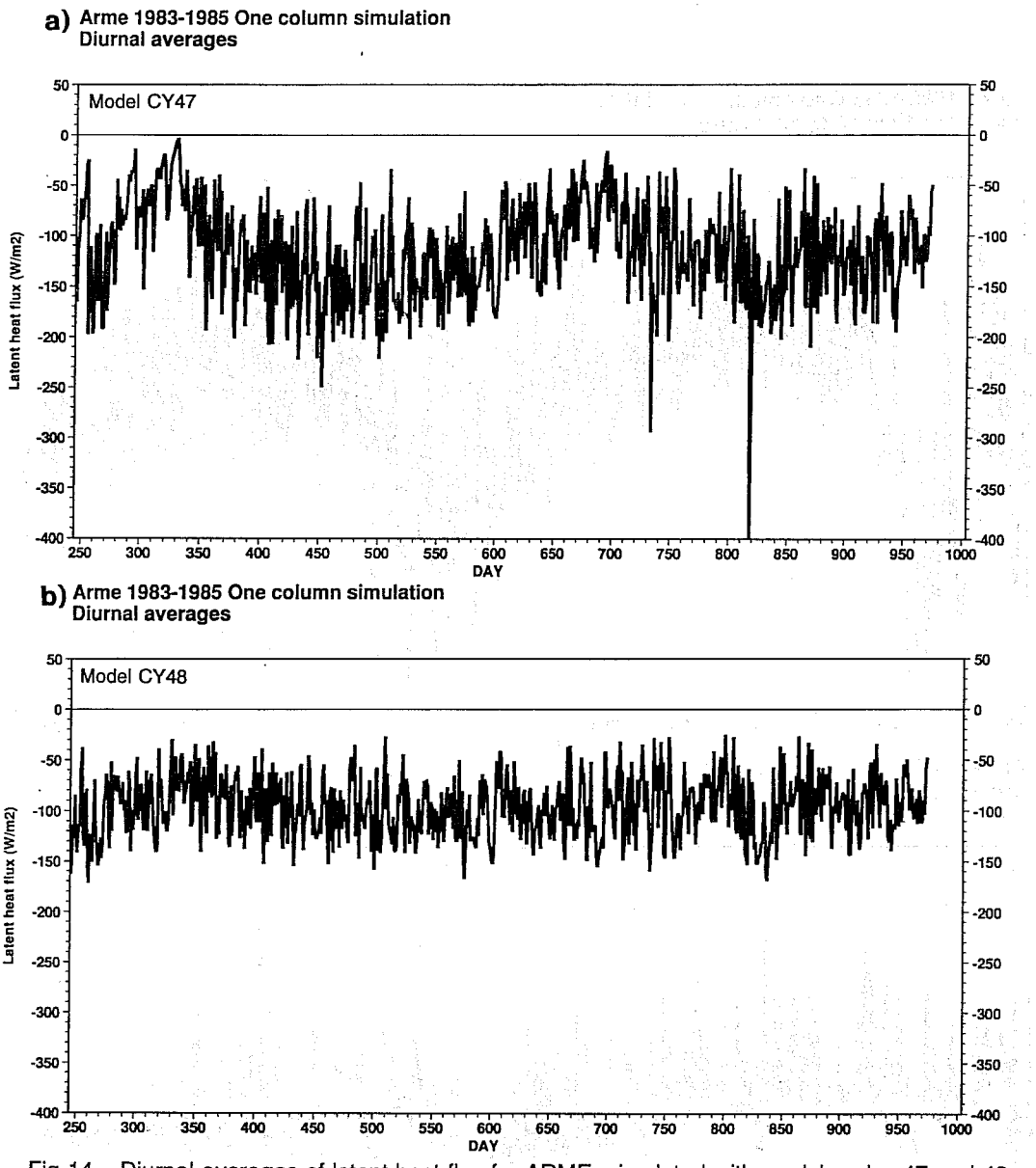

Fig 14 Diurnal averages of latent heat flux for ARME, simulated with model cycles 47 and 48.

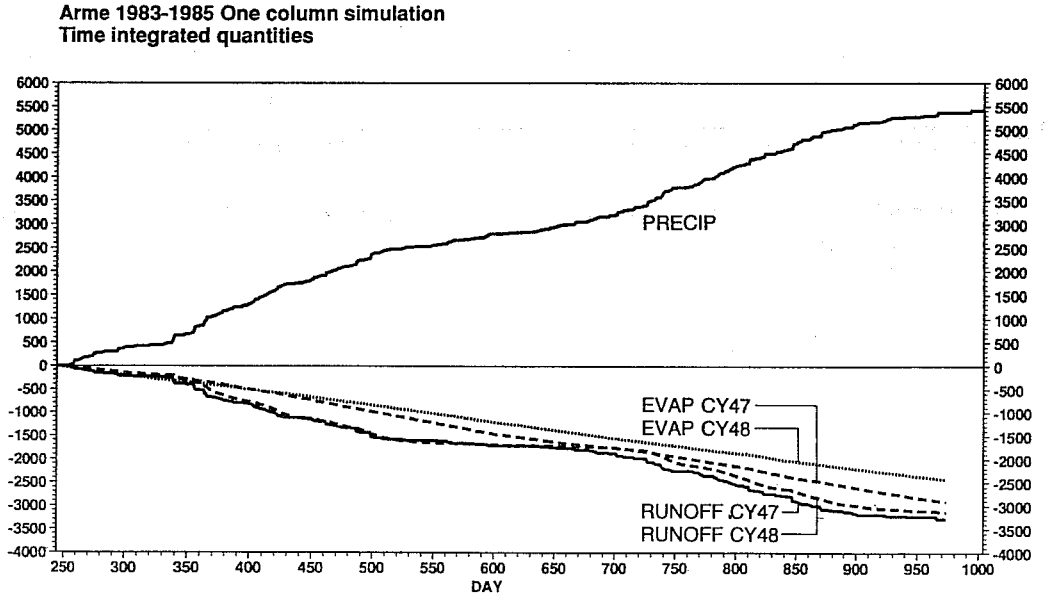

Fig 15 Accumulated moisture budget at the surface for ARME.

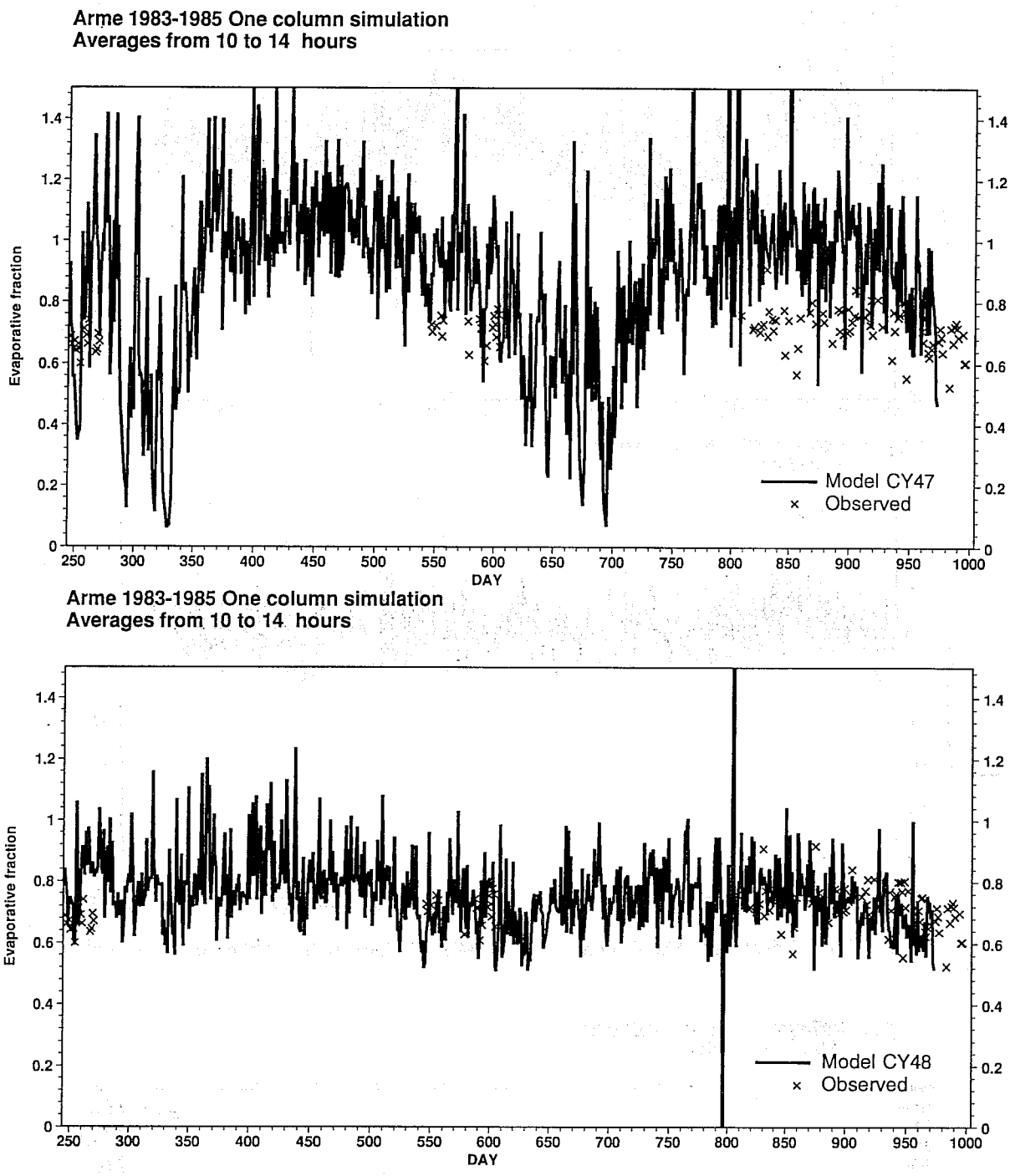

Fig 16 Midday evaporative fraction (averaged over 4 hours around local noon) for ARME with model cycles 47 and 48 in comparison with data.

although not all seasons have observations of the surface energy balance. The observations suggest an evaporative fraction of about 0.7 throughout the year. Model cycle 48 reproduces this value rather closely and has virtually no annual cycle. Apparently, the soil moisture reservoir is big enough to provide unlimited supply during the dry season.

Finally we compare accumulated interception with data by *Lloyd and Marques* (1988) in Fig 17. Both model cycles are well within the range of observational data. The accumulated evaporation with cycle 48 is also very close to the results from the Penman-Monteith-Rutter model (*Lloyd et al*, 1988; *Shuttleworth*, 1988). The latter is tuned to the ARME location, and uses the observed soil water tension in the stress function. Therefore it can be expected to give superior results to our two schemes and is used as a reference for the parametrization under test in this paper.

4. MULTIYEAR INTEGRATIONS WITH THE GLOBAL MODEL

The seasonal evolution of soil temperature and soil moisture in the ECMWF operational forecast system is the result of forcing from the 6 hour forecasts during the successive data assimilation cycles. The soil moisture content evolves as the result of precipitation and evaporation from 6 hour forecasts which are used as first guesses for the atmospheric fields. In cycle 47 the seasonal evolution is also (perhaps even mainly) affected by the deep boundary condition, which is updated every month. To test the seasonal time scales of the soil variables, it would be necessary to do a full year of data assimilation, which is very demanding in terms of computer resources. It was therefore decided to do a multiyear run (4.5 years in duration) with model cycles 47 and 48 at T63L31 resolution, mainly to see whether there is any model drift on the seasonal time scale. The sea surface temperatures vary throughout the year following a climate based on the averaged annual cycle of the years 1986-1991.

Here we present the mean annual cycle from these multiyear runs at the three different locations that have been used in the one column simulations. The inter annual variability can be considerable in the model as well in the observations, which makes for deficient comparisons with data obtained over one or two years only. On the other hand, the differences between the long run and the data are often larger and more systematic than the inter annual variability in the multiyear integration. It is therefore felt that the comparison with the data is a useful exercise. The model may also be biased in components of the general circulation which have impact on near surface parameters, but which cannot be attributed to land surface processes.

It is worth discussing the scales represented by the model values with the scales implied by the observations. For FIFE, which was a scale integration experiment, the heterogeneity is smaller than the model bias, as already pointed out in section 3a. The ARME data is from a point over tropical forest and this site is

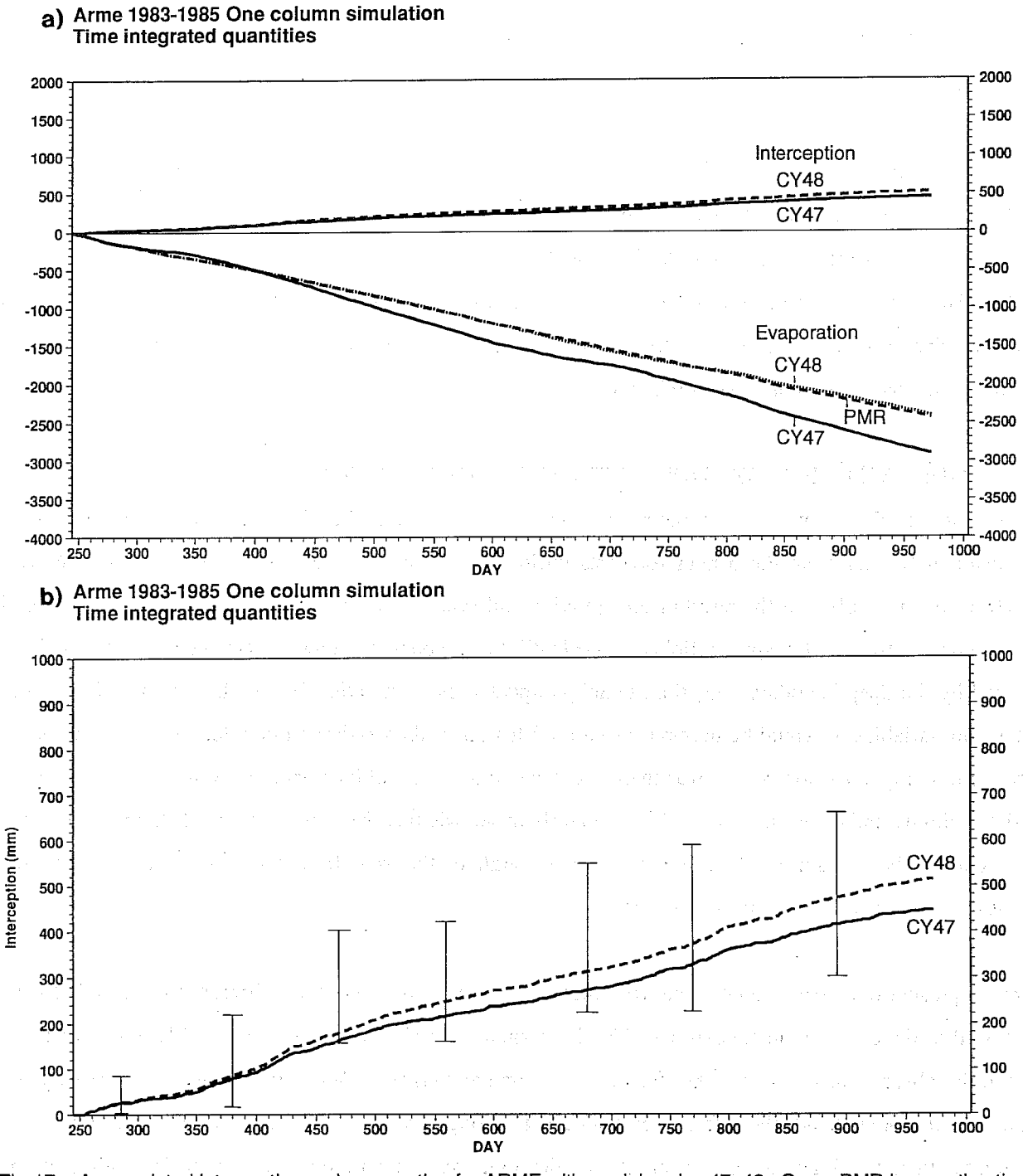

Fig 17 Accumulated interception and evaporation for ARME with model cycles 47, 48. Curve PMR is an estimation of evaporation from the Penman-Monteith-Rutter model as described by *Shuttleworth* (1988) with some improvements by *Dolman et al* (1991). The accumulated interception is repeated in Fig b - notice the different scale - in comparison with the range of observations (error bars) as published by *Sellers et al* (1989).

typical for very large areas surrounding the observation point. Also Cabauw is a typical site for the surrounding area. Compared to the model bias, we feel that for these three locations the problem of representativeness is of secondary scale.

To compare model with data, monthly mean values of different quantities have been computed for the locations discussed in section 3. To get a single annual cycle the model output for different years has been averaged month by month (4 years). The same has been done for the data. For FIFE only 4 full months exists, for Cabauw we have one year of monthly averages and for ARME 2 years and 1 month have been averaged to a single annual cycle.

The annual cycles of the two models are compared with data in Figs 18, 19, and 20 for FIFE, Cabauw and ARME respectively. For FIFE we only have data from June to September. We see that the downward solar radiation and the net radiation agree well with the data for these months. Cycle 48 is slightly better than cycle 47. However, the sensible heat flux is too large and the latent heat flux is too small in both versions of the model. The reason can be found in the soil moisture and the precipitation. The soil moisture is rather low throughout the year and precipitation is underestimated, with cycle 48 having less precipitation than cycle 47. The ground heat flux is smaller with cycle 48 particularly during the second half of the year when the fixed temperature boundary condition forces a rather unrealistic annual cycle. This improvement is due to the relaxation of the deep boundary condition and due to the introduction of a skin temperature (see also *Beljaars and Betts*, 1993 for a discussion of the impact of the skin temperature parametrization on the diurnal cycle of the ground heat flux).

For the Cabauw site the downward solar radiation and the net radiation at the surface are considerably overestimated by both model cycles, although cycle 48 is slightly better than cycle 47. This is consistent with results of operational verification indicating a systematic underestimation of cloud cover. The latent heat flux is quite reasonable particularly with cycle 48, but the sensible heat flux is poor with both model cycles. In summer both models produce far too much heating and in winter too much cooling. Precipitation is too high in winter and too low in summer with both models. The ground heat flux is slightly smaller with cycle 48 and has a better balance between summer and winter.

For ARME the available data is limited to solar downward radiation, net radiation, precipitation and latent heat flux estimates from the Penman-Monteith-Rutter model kindly provided by Dr John Gash from The Institute of Hydrology (*Lloyd et al*, 1988). This PMR model has been optimized for the ARME location and is therefore used as reference for the current model. Both our models (Cy47 and Cy48) overestimate the solar downward radiation and the net radiation. Also the latent heat flux is slightly overestimated, but this is most likely due to an overestimation of net radiation. The annual cycle of

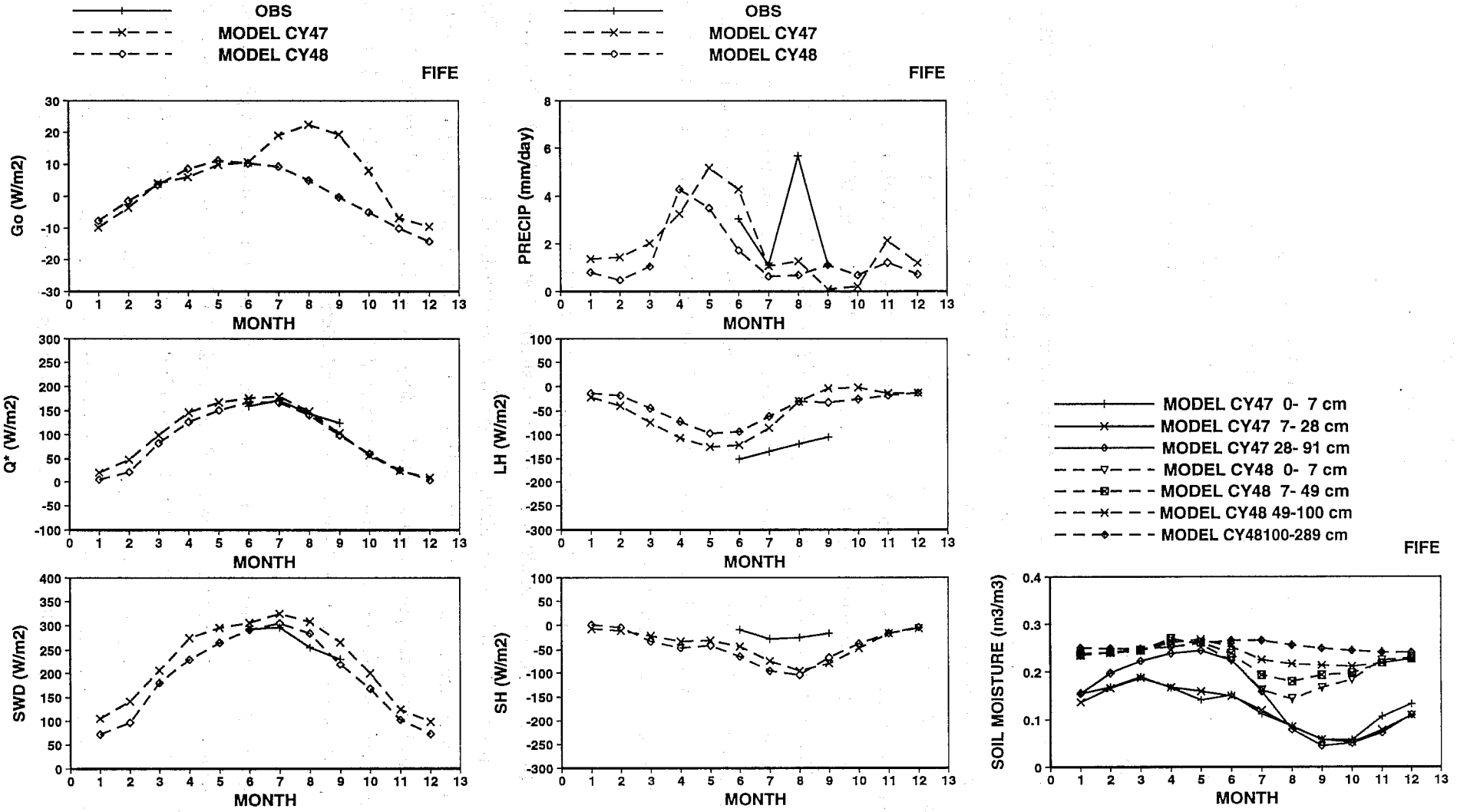

Fig 18 Annual cycles of monthly averages from the multiyear runs with cycle 47s and 48 at T63L31 resolution in comparison with data (if available) at the FIFE location. (a) Solar downward radiation, (b) Net total radiation, (c) Ground heat flux, (d) Sensible heat flux, (e) Latent heat flux, (f) Precipitation and (g) Soil moisture in the three layers of cycle 47 and the four layers of cycle 48.

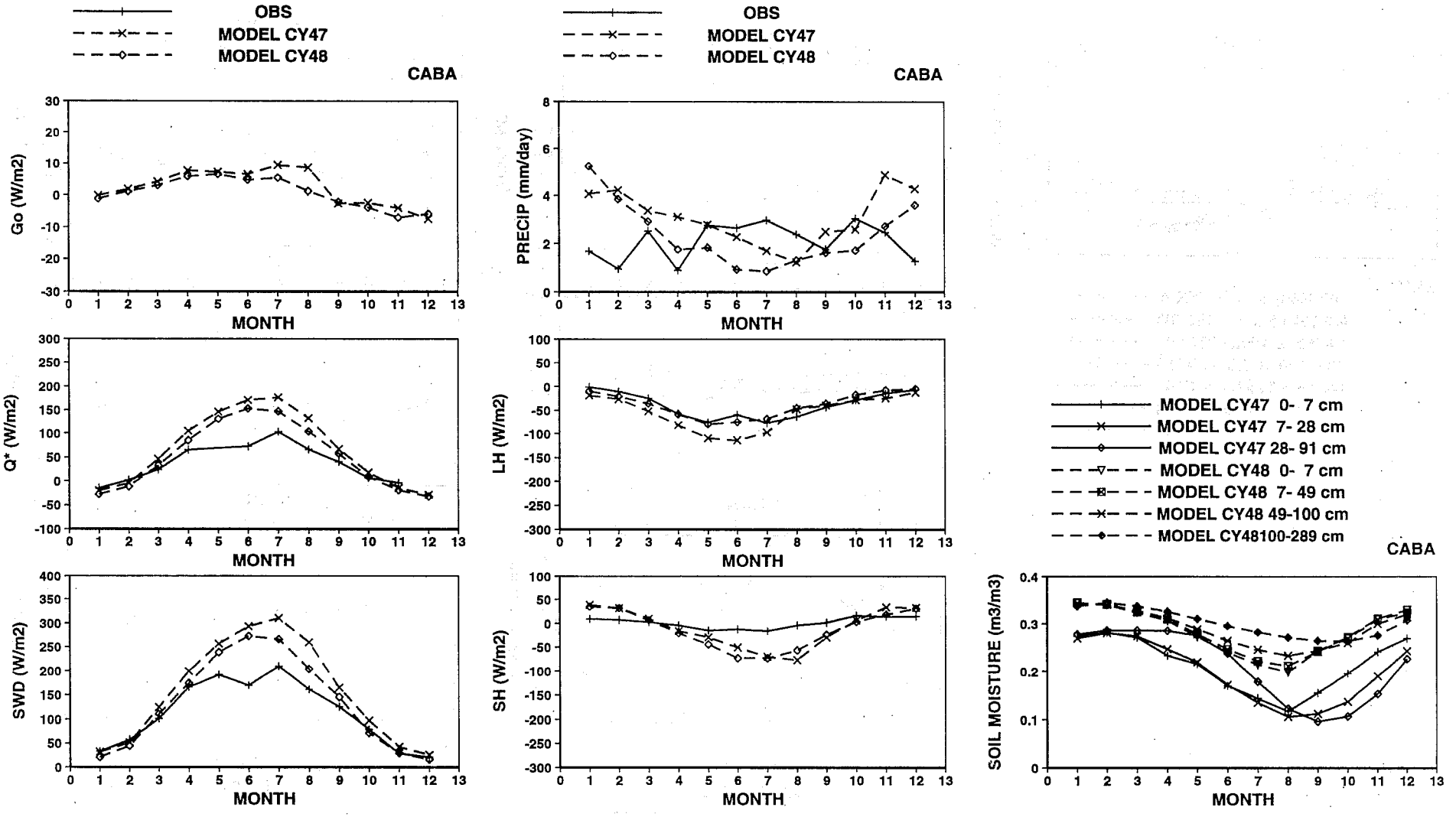

Fig 19 As Fig 18 for Cabauw

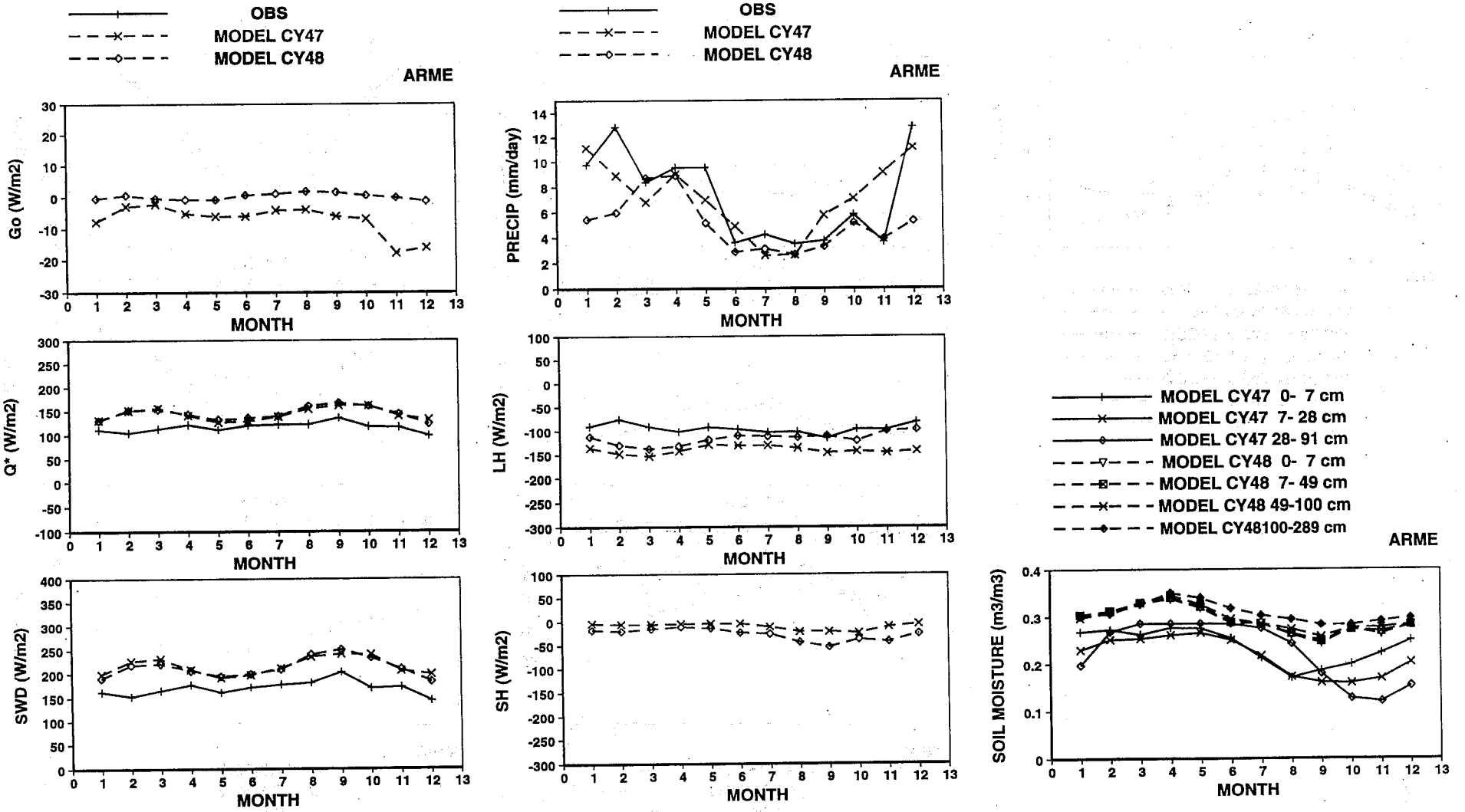

Fig 20 As Fig 18 for ARME

precipitation looks reasonable. The ground heat flux is small with cycle 48 throughout the year whereas cycle 47 has a systematic flux from the climate layer, because its temperature is not in equilibrium with the model climate.

Prior to operational implementation of model cycle 48, it was concluded from the multiyear runs that no dramatic drift occurred. However, the annual cycles for the 3 locations show a very mixed signal. Cycle 48 is sometimes better than cycle 47 and vice-versa. The main reason is that precipitation and the surface radiation respond in very complicated ways to the model changes. The changes seen in the verification in climate mode are dominated by the changes in surface radiation and precipitation rather then by the direct effects of the changes in land surface parametrization. Therefore it would be extremely difficult to decide from these long runs which of the two parametrizations is the best. The response of precipitation and radiation to changes in the land surface parametrization prevents us from drawing firm conclusions. A clear example of interactions of the land surface with the boundary layer structure and moist convection was obtained in recent work, where the effect of the new land surface parametrization on the precipitation over the USA is discussed (A K Betts, personal communication). Given these complicated interactions, it is felt that the stand-alone one column simulations are extremely useful because they allow one to separate the issue of land surface parametrization from other model problems.

5. SUMMARY AND CONCLUSIONS

A new version of the ECMWF land surface scheme has been described. The main difference with the old scheme is a more physical representation of the soil hydrology. A typical feature of the old scheme is its rapid relaxation towards a climatologically prescribed deep boundary condition for temperature and soil moisture. The new scheme has four prognostic layers with free drainage of water and a zero flux condition for heat at the bottom. Hydraulic diffusivity and conductivity are strongly dependent on soil moisture, allowing a rapid downward transport of water after rainfall events. The soil water holding capacity of the new model is large enough in order to maintain evaporation during the dry season, for the datasets tested. Interception of precipitation is included, and the evaporation rate is different for bare ground, dry vegetation and wet vegetation. The roughness length for heat and moisture is different from its value for momentum. Finally, a skin temperature is considered, representing the response of a thin top surface layer, in instantaneous equilibrium with its forcing.

The emphasis of this paper is on the seasonal time scale and on validation in stand-alone mode using long observational time series. The study of the seasonal time scale in land surface schemes is relatively new as it requires continuous observations of fluxes and soil variables over long periods of time (*Henderson-Sellers et al*, 1993). However, the seasonal time scales, mainly determined by the soil moisture reservoir, are crucial to climate and numerical weather prediction models (*Manabe*, 1969; *Milly and Dunne*,

1994). Long datasets are now becoming available and we have used them to test two versions of the ECMWF land surface parametrization scheme. It is clear that the new prognostic scheme has a much better capability for handling seasonal anomalies in stand-alone mode than the old model, which is heavily constrained by a deep soil climate boundary condition.

The different observed datasets illustrate different aspects of the two models. The FIFE dataset (prairie grass) has two extended periods of drying which are poorly handled by the old model. The old model produces far too much runoff because the downward diffusion of water between layer one and layer two is too slow, resulting in large saturation runoff from layer one. Because of the quick loss of precipitation and the too dry climatological deep boundary condition, the old model has too little evaporation during dry spells. The new model has conductivities and diffusivities that are strongly dependent on soil moisture, which allows a rapid downward transport of water after precipitation. Therefore the new model has more soil moisture available for evaporation during dry spells. Although the evaporation in the new model is much closer to the observed evaporation during the dry spells, there is still an underestimation. This may be due to a mismatch between soil type of the model (we use one type for the entire globe) and the soil type in the FIFE area, which has a slightly larger water holding capacity than the model.

The Cabauw dataset (grassland) represents a very different climatological regime. The precipitation comes at moderate rates throughout the year and therefore evaporation is only rarely supply limited. For Cabauw, the formulation of aerodynamic resistance turns out to be important, particularly in winter when the vegetation is wet for long periods of time. The new model has a reduced roughness length for heat and moisture which increases the aerodynamic resistance and therefore reduces evaporation. The new model agrees better with observations than the old model.

For ARME (tropical forest) the old model has a distinct annual cycle in the midday evaporative fraction, which is forced by the deep soil climatological boundary condition. Observations suggest a constant evaporative fraction of 0.7 for all seasons. The new model has sufficient water capacity in the soil to maintain evaporation during the dry season. The interception loss is well within the regime of observational uncertainty with both schemes.

This study clearly demonstrates the importance of observational data to test different aspects of the parametrization. We feel that stand-alone validation is the only way to isolate deficiencies of the land surface parametrization from other model deficiencies. This became particularly evident from a comparison of the old and new scheme in a multiyear run of the global model. From the annual cycles at the different locations, it was difficult to decide which scheme performed best. The reason is that evaporation interacts with precipitation in a complicated way. An example is given in recent work, suggesting that a non-local

response to soil moisture affected the short range precipitation forecasts in the ECMWF model in July 1993 over the USA (A K Betts, personal communication).

The datasets that have been used were very important for the validation of our new surface scheme, and in fact very helpful in testing the code. The seasonal time scale is underrepresented in observational studies. The FIFE experiment had more emphasis on scale aggregation aspects and diurnal cycles than on the seasonal time scale. The drying phases occurred between the IFC's and were documented by two flux stations only. Nevertheless FIFE is one of the very few experiments for which extensive observations of soil moisture exists. The FIFE neutron probe data has unfortunately not been used much and a study of the quality of the data and the origin of the mismatch between soil moisture evolution and precipitation-evaporation difference would be most welcome.

A number of issues are still unresolved in soil parametrization and should be addressed from the observational point of view. The most important parameter is the total size of the soil moisture reservoir: how much water can the soil hold and make available for evaporation later. The rooting depth and soil properties affect this parameter. In spite of its importance (*Patterson*, 1990; *Milly and Dunne*, 1994), very few observational field studies are dedicated to the soil water holding capacity. It is also not very clear how the soil moisture profile controls the surface resistance of the vegetation. We have adopted a simple arithmetic average of the soil moisture over the three top soil layers covering a depth of 1 m and a linear stress function. The resulting soil moisture profiles show qualitative agreement with observed profiles during FIFE, but observations tend to be much dryer near the surface without apparent impact on evaporation. The observed profiles suggest a gradual soil moisture depletion from top to bottom, with very little change in stress on the plants similar to the findings by *Federer* (1979). It is not very clear how to parametrize this effect in detail.

The one-dimensional validation presented in section 3 of this paper has shown that the surface model is realistic when the correct forcing is imposed. This does not guarantee that the model will perform correctly when introduced in a GCM, where the forcing is defined at every time step by the atmospheric component. Errors in the shortwave surface radiation and precipitation can induce soil moisture anomalies which might feed back on the atmosphere. One such feedback might occur if there is excessive solar radiation at the surface, due e.g. to a deficiency in the model clouds. This then leads to a drying out of the surface, and thus too little precipitation and cloud cover. The problem can be aggravated in numerical weather prediction: since there are currently no routine global observations of soil moisture in the root zone, the model has to run with initial values of soil moisture from a very short-range forecast, representing a balance between precipitation and evaporation. The only way to minimize the effect of these feedback loops is to initialise the soil moisture. For instance, *Bouttier et al* (1993a, 1993b) describe a scheme that relates

increments in soil moisture to errors in the short range forecast of 2 metre temperature and dewpoint. The new surface model described in this paper has been running operationally at ECMWF since August 1993. The feedback described above was encountered in the operational results over Europe, for the months of April/May/June 1994. We are currently working on a simple method to initialise the soil water in the root zone.

Acknowledgements

The validation exercise described in this paper would not have been possible without the generous support of a number of a experimental groups. The continuous surface flux dataset for FIFE was made available by Dr E A Smith of Florida State University; Drs A K Betts and J K Ball prepared the area averages from surface stations; the soil moisture profiles were processed from the FIFE-CDROM (*Stubel et al*, 1991). The ARME data was made available by the Institute of Hydrology and collected as part of a collaborative experiment between the UK Natural Environment Research Council (NERC) and the Brazilian Conselho Nacional de Desenvolvimento Cientifico and Technologico (CNPq). Dr J H C Gash provided the output of the Penman-Monteith-Rutter model for ARME. The Cabauw data was made available by the Royal Netherlands Meteorological Institute (KNMI) for which we particularly thank Mr G van der Vliet. We thank Dr A K Betts, from Atmospheric Research, and Dr J Noilhan from Centre National de Recherches Meteorologiques (CNRM, France) for the advice and encouragement they gave on a number of aspects of the new parametrization during short visits at ECMWF. Mr B van der Hurk, from Wageningen University, our colleagues at ECMWF, Drs Tony Hollingsworth, Martin Miller and Adrian Simmons, and two anonymous referees gave valuable suggestions for improvement to the manuscript.

References

Abramopoulos, F, C Rosenzweig and B Choudury, 1988: Improved ground hydrology calculations for global climate models (GCMs): Soil water movement and evapotranspiration. J Climate, **1**, 921-941.

Beljaars, A C M, 1995: The parametrization of surface fluxes in large scale models under free convection. Quart J Roy Meteor Soc, **121**, 255-270.

Beljaars, A C M and A K Betts, 1993: Validation of the boundary layer scheme in the ECMWF model. Proc Seminar ECMWF, 7-11 September 1992. Reading, UK, ECMWF, Vol II, 159-195.

Beljaars, A C M and A A M Holtslag, 1990: A software library for the calculation of surface fluxes over land and sea, Environm Softw, **5**, 60-68.

Beljaars, A C M and A A M Holtslag, 1991: Flux parametrization over land surfaces for atmospheric models. J Appl Meteor, **30**, 327-341.

Beljaars, A C M and P Viterbo, 1994: The sensitivity of winter evaporation to the formulation of aerodynamic resistance in the ECMWF model. Bound-Layer Meteor, **71**, 135-149.

Betts, A K and J H Ball, 1992: FIFE-1987 mean surface time series, Data diskette, Atmospheric Research, Pittsford, VT 05763.

Betts, A K, J H Ball and A C M Beljaars, 1993: Comparison between the land surface response of the ECMWF model and the FIFE-1987 data. Quart J Roy Meteor Soc, **119**, 975-1001.

Betts, A K and A C M Beljaars, 1993: Estimation of effective roughness length for heat and momentum from FIFE data. Atmos Res, **30**, 251-261.

Blondin, C, 1991: Parametrization of land-surface processes in numerical weather prediction. Land surface evaporation: Measurement and parametrization, T J Schmugge and J-C André, Eds, Springer, 31-54.

Bouttier, F, J-F Mahfouf and J Noilhan, 1993a: Sequential assimilation of soil moisture from atmospheric low-level parameters. Part I: Sensitivity and calibration studies. J Appl Meteor, **32**, 1335-1351.

Bouttier, F, J-F Mahfouf and J Noilhan, 1993b: Sequential assimilation of soil moisture from atmospheric low-level parameters. Part II: Implementation in a mesoscale model. J Appl Meteor, **32**, 1352-1364.

Brutsaert, W, 1982: Evaporation into the atmosphere. D Reidel, 299 pp.

Carlson, T N, 1991: Recent advances in modeling the infrared temperature of vegetation canopies. Land surface evaporation: Measurement and parametrization, T J Schmugge and J-C André, Eds, Springer, 349-358.

Clapp, R B and G M Hornberger, 1978: Empirical equations for some soil hydraulical properties. Water Resour Res, **14**, 601-604.

Cosby, B J, G M Hornberger, R B Clapp and T R Ginn, 1984: A statitistical exploration of the relationships of soil moisture characteristics to the physical properties of soils. Water Resour Res, **20**, 682-690.

de Vries, D A, 1975: Heat transfer in soils. Heat and mass transfer in the biosphere. Part1: Transfer processes in the plant environment, D A de Vries and N H Afgan, Eds, Wiley, 4-28.

Deardorff, J W, 1978: Efficient prediction of ground surface temperature and moisture, with inclusion of a layer of vegetation. J Geophys Res, **83C**, 1889-1903.

Delworth, T L and S Manabe, 1988: The influence of potential evaporation on the variabilities of simulated soil wetness and climate. J Climate, **1**, 523-547.

Delworth, T L and S Manabe, 1989: The influence of soil wetness on near-surface atmospheric variability. J Climate, **2**, 1447-1462.

Dickinson, R E, 1984: Modeling evapotranspiration for three-dimensional climate models. Climate processes and climate sensitivity. Geophys Monogr, No. 29, Amer Geophys Union, 58-72.

Dickinson, R E, 1988: The force-restore model for surface temperatures and its generalizations. J Climate, **1**, 1086-1097.

Dickinson, R E, A Henderson-Sellers, P J Kennedy and M F Wilson, 1986: Biosphere-atmosphere transfer scheme (BATS) for the NCAR community model. NCAR Technical Note, NCAR/TN-275+STR, 69pp.

Dickinson, R E, A Henderson-Sellers, C Rosenzweig and P J Sellers, 1991: Evapotranspiration models with canopy resistance for use in climate models, a review. Agric Forest Meteor, **54**, 373-388.

Dolman, A J, J H C Gash, J Roberts and W J Shuttleworth 1991: Stomatal and surface conductance of tropical rainforest. Agric Forest Meteor, **54**, 303-318.

Dolman, A J and D Gregory, 1992: The parametrization of rainfall interception in GCMs. Quart J Roy Meteor Soc, **118**, 445-467.

Driedonks, A G M, H van Dop and W Kohsiek, 1978: Meteorological observations on the 213 m mast at Cabauw in the Netherlands. Preprints, 4th Symp Meteor Observ and Instrum, Denver, USA, Amer Meteor Soc, 41-46.

Famiglietti, J S, E F Wood, M Sivapalan and D J Thongs, 1992: A catchment scale water balance model for FIFE. J Geoph Res, **97D**, 18997-19007.

Federer, C A, 1979: A soil-plant-atmosphere model for transpiration and availability of soil water. Water Resour Res, **15**, 555-562.

Garratt, J R, 1993: Sensitivity of climate simulations to land-surface and atmospheric boundary layer treatments - A review. J Climate, **6**, 419-449.

Goutorbe, J-P, J Noilhan, C Valancogne and R H Cuenca, 1989: Soil moisture variations during HAPEX-MOBILHY. Ann Geophys, **7**, 415-426.

Henderson-Sellers, A, Z-L Yang and R E Dickinson, 1993: The project for intercomparison of land-surface parametrization schemes. Bull Amer Meteor Soc, **74**, 1335-1349.

Hillel, D, 1982: Introduction to soil physics. Academic Press, 368 pp.

Holtslag, A A M and A P van Ulden, 1983: A simple scheme for daytime estimates of the surface fluxes from routine weather data. J Clim Appl Meteor, **22**, 517-529.

Jarvis, P G, 1976: The interpretation of the variations in leaf-water potential and stomatal conductance found in canopies in the field. Phil Trans Roy Soc London, **B723**, 593-610.

Kim, J and S B Verma, 1990: Components of surface energy balance in a temperature grassland ecosystem. Bound-Layer Meteor, **51**, 401-417.

Kondo, J, N Saigusa and T Sato, 1990: A parametrization of evaporation from bare soil surfaces. J Appl Meteor, **29**, 385-389.

Lloyd, C R, J H C Gash, W J Shuttleworth and A de O Marques, 1988: The measurement and modelling of rainfall interception by Amazonian rain forest. Agr Forest Meteor, **43**, 277-294.

Lloyd, C R and A de O Marques, 1988: Spatial variability of throughfall and stemflow measurements in Amazonian rainforest. Agr Forest Meteor, **42**, 63-73.

Louis, J F, 1979: A parametric model of vertical eddy fluxes in the atmosphere. Bound-Layer Meteor, **17**, 187-202.

Mahfouf, J F and B Jacquemin, 1989: A study of rainfall interception using a land surface parametrization for mesoscale meteorological models. J Appl Meteor, **28**, 1282-1302.

Mahfouf, J F and J Noilhan, 1991: Comparative study of various formulations from bare soil using in situ data. J Appl Meteor, **30**, 1354-1365.

Mahrt, L and H-L Pan, 1984: A two-layer model of soil hydrology. Bound-Layer Meteor, **29**, 1-20.

Manabe, S, 1969: Climate and the ocean circulation, 1. The atmospheric circulation and the hydrology of the earth's surface. Mon Wea Rev, **97**, 739-774.

McCumber, M and R A Pielke, 1981: Simulation of the effects of surface fluxes of heat and moisture in a mesoscale numerical model. 1. Soil layer. J Geophys Res, **86C**, 9929-9938.

Milly, P C D, 1982: Moisture and heat transport of hysteretic, inhomogeneous porous media: A matric head-based formulation and a numerical model. Water Resour Res, **18**, 489-498.

Milly, P C D and K A Dunne, 1994: Sensitivity of the global water cycle to the water-holding capacity of land. J Climate, **7**, 506-526.

Mintz, Y, 1984:The sensitivity of numerically simulated climates to land-surface boundary conditions. Global Climate. J Houghton, Ed, CUP, 79-105.

Mintz, Y and Y V Serafini, 1992: A global monthly climatology of soil moisture and water balance, Climate Dyn, **8**, 13-27.

Namias, J, 1958: Persistence of mid-tropospheric circulations between adjacent months and seasons. The atmosphere and sea in motion (Rossby memorial volume). B Bolin, Ed, Rockefeller Institute Press, 240-248.

Noilhan, J and S Planton, 1989: A simple parametrization of land surface processes for meteorological models. Mon Wea Rev, **117**, 536-549.

Patterson, K A, 1990: Global distribution of total and total-available soil water-holding capacities. Msc Thesis, Univ of Delaware, 119 pp.

Pitman, A J, A Henderson-Sellers, F Abramopoulos, R Avissar, G Bonan, A Boone, J G Cogley, R E Dickinson, M Ek, D Entekhabi, J Famiglietti, J R Garratt, M Frech, A Hahmann, R Koster, E Kowalczyk, K Laval, L Lean, T J Lee, D Lettenmaier, X Liang, J-F Mahfouf, L Mahrt, C Milly, K Mitchell, N de Noblet, J Noilhan, H Pan, R Pielke, A Robock, C Rosenzweig, S W Running, A Schlosser, R Scott, M Suarez, S Thompson, D Verseghy, P Wetzel, E Wood, Y Xue, Z-L Yang and L Zhang, 1993: Results from the off-line control simulation phase of the Project for Intercomparison of Landsurface Parametrization Schemes (PILPS). IGPO Publ Series, 7, 47 pp.

Philip, J R, 1957: Evaporation, and moisture and heat fields in the soil. J Meteor., **14**, 354-366.

Richards, L A, 1931: Capillary conduction of liquids through porous mediums. Physics, **1**, 318-333.

Richtmyer, R D and K W Morton, 1967: Difference methods for initial value problems. Interscience, 406 pp.

Rutter, A J, K A Kershaw, P C Robins and A J Morton, 1972: A predictive model of rainfall interception in forests. I. Derivation of the model from observations in a plantation of Corsican pine. Agric Meteor, **9**, 367-384.

Rutter, A J, A J Morton and P C Robins, 1975: A predictive model of rainfall interception in forests. II. Generalization of the model and comparison with observations in some coniferous and hardwood stands. J Appl Ecol, **12**, 367-380.

Sausen, R, S Schubert and L Dümenil, 1994: A model of river runoff for use in coupled atmosphere-ocean models. J Hydrol, **155**, 337-352.

Sellers, P J, 1985: Canopy reflectance, photosynthesis and transpiration. Int J Remote Sens, **6**, 1335-1372.

Sellers, P J, F G Hall, G Asrar, D E Strebel and R E Murphy, 1988: The first ISLSCP field experiment (FIFE). Bull Amer Meteor Soc, **69**, 22-27.

Sellers, P J, Y Mintz, Y C Sud and A Dalcher, 1986: A simple biosphere model (SiB) for use within general circulation models. J Atmos Sci, **43**, 505-531.

Sellers, P J, W J Shuttleworth, J L Dorman, A Dalcher and J M Roberts 1989: Calibrating the Simple Biosphere model for Amazonian tropical rainforest using field and remote sensing data. Part I: Average calibration with field data. J Appl Meteor, **28**, 727-759.

Shuttleworth, W J, 1988: Evaporation from Amazonian rainforest, Proc Roy Soc London, **B233**, 321-346.

Shuttleworth, W J, J H C Gash, C R Lloyd, C J Moore, J Roberts, A O Marques, G Fisch, V P Silva, M N G Ribeiro, L C B Molion, L D A Sá, J C Nobre, O M R Cabral, S R Patel and J C Moraes, 1984a: Eddy correlation measurements of energy partition for Amazonian forest. Quart J Roy Meteor Soc, **110**, 1143-1162.

Shuttleworth, W J, J H C Gash, C R Lloyd, C J Moore, J Roberts, A O Marques, G Fisch, V P Silva, M N G Ribeiro, L C B Molion, L D A Sá, J C Nobre, O M R Cabral, S R Patel and J C Moraes, 1984b: Observations of radiation exchange above and below Amazonian forest. Quart J Roy Meteor Soc, **110**, 1163-1169.

Smith, E A, W L Crosson and B D Tanner, 1992: Estimation of surface heat and moisture fluxes over a prairie grassland; 1. In situ energy budget measurements incorporating a cooled mirror dew hygrometer. J Geophys Res, **97**, 18557-18582.

Strubel, D E, D Landis, J A Newcomer, J DeCampo and B W Meeson 1991: Collected data of the First ISLSCP Field Experiment. Prototype volume, Published on CDROM by NASA.

Viterbo, P and L Illari, 1994: The impact of changes in the runoff formulation of a general circulation model on surface and near-surface parameters. J Hydrol, **115**, 325-336.

Wang, J R, 1992: An overview of measurements of soil moisture and modeling of moisture flux in FIFE. J Geophys Res, **97D**, 18955-18959.

Warrilow, D L, A B Sangster and A Slingo, 1986: Modelling of land-surface processes and their influence on European climate. UK Met Office Rep, Met O 20, Tech Note No. 38, 92 pp.

Wilson, M F and A Henderson-Sellers, 1985: A global archive of land cover and soil data sets for use in general circulation climate models. J Climatol, **5**, 119-143.

Wilson, M F, A Henderson-Sellers, R E Dickinson and P J Kennedy, 1987: Sensitivity of the biosphere-atmosphere transfer scheme (BATS) to the inclusion of variable soil characteristics. J Climate Appl Meteor, **26**, 341-362.

Xue, Y, P J Sellers, J L Kinter and J Shukla, 1991: A simplified biosphere model for global climate studies. J Climate, **4**, 345-364.

Appendix

The "old" ECMWF surface model (Cycle 47)

The previous ECMWF surface model is described in *Blondin* (1991). For ease of interpretation of the comparison between the old and the new model, we present in this appendix a brief description of the old model, emphasizing the differences between the two model versions.

The old model discretizes the soil in two active layers plus one additional layer underneath, with specified, monthly-varying fields of soil moisture and temperature, acting as lower boundary conditions. The depths of the model layers are

D_1= 0.07 m, D_2= 0.42 m, D_3= 0.42 m

On top of the soil layers there is an interception reservoir, with properties described in sections 2c and 2d. No skin temperature is used.

The soil heat budget follows

$$\frac{(\rho C)}{\Delta t}(T_i^{n+1} - T_i^n) = -\frac{(G_{i,b} - G_{i,t})}{D_i} \qquad i=1,2$$

where $G_{i,b}$, $G_{i,t}$ are the heat fluxes (positive downwards, units Wm^{-2}) at the bottom and at the top of layer i, respectively, defined as:

$$G_{i,b} = -\lambda_T \frac{T_{i+1}^n - T_i^{n+1}}{0.5(D_i + D_{i+1})} \qquad i=1,2$$

$$G_{i,t} = -\lambda_T \frac{T_i^{n+1} - T_{i-1}^n}{0.5(D_{i-1} + D_i)} \qquad i=2$$

The constants for soil heat capacity ρC and thermal conductivity λ_T have the numerical values 2.4×10^6 $Jm^{-3}K^{-1}$ and 1.57 $Wm^{-3}K^{-1}$, respectively. T_3, the bottom boundary condition, is a monthly climatology. Top boundary condition is specified by $G_{1,t}$, the sum of sensible plus latent heat plus the net radiation.

The sensible heat flux and evaporation follow equations (7), but the roughness length for heat and momentum are identical, stability is specified in terms of a Richardson number dependency, rather than an Obukhov length (*Louis*, 1979), and the top soil temperature T_1, replaces the skin temperature, T_{sk}. The treatment of evaporation follows the description of section 2c, with some changes: In equation(20), the constant 1.6 is replaced by unity and the water at field capacity is used instead of the saturation value,

r_{smin}=100 sm^{-1} (compared to 240 sm^{-1} used by the new model), and the root profile is specified by R_1=R-2=0.5, R_3=0.

The soil water budget of the two soil layers follows equations similar to (30)-(32), but with constant values of hydraulic diffusivity and conductivity, given by $\lambda=10^{-7}$ m^2s^{-1} and $\gamma=10^{-10}$ ms^{-1}. Note that these values correspond to the values of the new coefficients for the lower third of availability. Other values for soil water properties are θ_{pwp}=0.086 m^3m^{-3}, θ_{cap}=0.171 m^3m^{-3}, and θ_{sat}=0.286 m^3m^{-3}. The flux at the bottom of the second layer is computed based on a lower soil water boundary condition given by the climatology of *Mintz and Serafini* (1992).

Runoff has three components: i) saturation excess, ii) a component due to sloping terrain, dependent on a variance of subgrid orography, and iii) the third component, when the precipitation exceeds a maximum infiltration limit, dependent on the water content of the top soil layer (see also *Viterbo and Illari*, 1994).

LIST OF ECMWF TECHNICAL REPORTS

1	A case study of a ten day forecast. (1976)	Arpe, K., L. Bengtsson, A. Hollingsworth, and Z. Janjić
2	The effect of arithmetic precision on some meteorological integrations. (1976)	Baede, A.P.M., D. Dent, and A. Hollingsworth
3	Mixed-radix Fourier transforms without reordering. (1977)	Temperton, C.
4	A model for medium range weather forecasts - adiabatic formulation. (1977)	Burridge, D.M., and J. Haseler
5	A study of some parameterisations of sub-grid processes in a baroclinic wave in a two dimensional model. (1977)	Hollingsworth, A.
6	The ECMWF analysis and data assimilation scheme: analysis of mass and wind field. (1977)	Lorenc, I. Rutherford and G. Larsen
7	A ten-day high-resolution non-adiabatic spectral integration; a comparative study. (1977)	Baede, A.P.M., and A.W. Hansen
8	On the asymptotic behaviour of simple stochastic-dynamic systems. (1977)	Wiin-Nielsen, A.
9	On balance requirements as initial conditions. (1978)	Wiin-Nielsen, A.
10	ECMWF model parameterisation of sub-grid scale processes. (1979)	Tiedtke, M., J.-F. Geleyn, A. Hollingsworth, and J.-F. Louis
11	Normal mode initialization for a multi-level grid-point model. (1979)	Temperton, C., and D.L. Williamson
12	Data assimilation experiments. (1978)	Seaman, R.
13	Comparison of medium range forecasts made with two parameterisation schemes. (1978)	Hollingsworth, A., K. Arpe, M. Tiedke, M. Capaldo, H. Sävijärvi, O. Åkesson, and J.A. Woods
14	On initial conditions for non-hydrostatic models. (1978)	Wiin-Nielsen, A.C.
15	Adiabatic formulation and organization of ECMWF's spectral model. (1979)	Baede, A.P.M., M. Jarraud, and U. Cubasch
16	Model studies of a developing boundary layer over the ocean. (1979)	Økland, H.
17	The response of a global barotropic model to forcing by large scale orography. (1980)	Quiby, J.
18	Confidence limits for verification and energetic studies. (1980)	Arpe, K.
19	A low order barotropic model on the sphere with orographic and newtonian forcing. (1980)	Källén, E.
20	A review of the normal mode initialization method. (1980)	Du Xing-yuan
21	The adjoint equation technique applied to meteorological problems. (1980)	Kontarev, G.
22	The use of empirical methods for mesoscale pressure forecasts. (1980)	Bergthorsson, P.
23	Comparison of medium range weather forecasts made with models using spectral or finite difference techniques in the horizontal. (1981)	Jarraud, M., C. Girard, and U. Cubasch

24	On the average errors of an ensemble of forecasts. (1981)	Derome, J.
25	On the atmospheric factors affecting the Levantine Sea. (1981)	Ozsoy, E.
26	Tropical influences on stationary wave motion in middle and high latitudes. (1981)	Simmons, A.J.
27	The energy budgets in North America, North Atlantic and Europe based on ECMWF analysis and forecasts. (1981)	Sävijärvi, H.
28	An energy and angular momentum conserving finite-difference scheme, hybrid coordinates and medium range weather forecasts. (1981)	Simmons, A.J., and R. Strüfing
29	Orographic influences on Mediterranean lee cyclogenesis and European blocking in a global numerical model. (1982)	Tibaldi, S. and A. Buzzi
30	Review and re-assessment of ECNET - A private network with open architecture. (1982)	Haag, A., Königshofer, F. and P. Quoilin
31	An investigation of the impact at middle and high latitudes of tropical forecast errors. (1982)	Haseler, J.
32	Short and medium range forecast differences between a spectral and grid point model. An extensive quasi-operational comparison. (1982)	Girard, C. and M. Jarraud
33	Numerical simulations of a case of blocking: The effects of orography and land-sea contrast. (1982)	Ji, L.R., and S. Tibaldi
34	The impact of cloud track wind data on global analyses and medium range forecasts. (1982)	Kållberg, P., S. Uppala, N. Gustafsson, and J. Pailleux
35	Energy budget calculations at ECMWF. Part 1: Analyses 1980-81. (1982)	Oriol, E.
36	Operational verification of ECMWF forecast fields and results for 1980-1981. (1983)	Nieminen, R.
37	High resolution experiments with the ECMWF model: a case study. (1983)	Dell'Osso, L.
38	The response of the ECMWF global model to the El-Niño anomaly in extended range prediction experiments. (1983)	Cubasch, U.
39	On the parameterisation of vertical diffusion in large-scale atmospheric models. (1983)	Manton, M.J.
40	Spectral characteristics of the ECMWF objective analysis system. (1983)	Daley, R.
41	Systematic errors in the baroclinic waves of the ECMWF. (1984)	Klinker, E., and M. Capaldo
42	On long stationary and transient atmospheric waves. (1984)	Wiin-Nielsen, A.C.
43	A new convective adjustment. (1984)	Betts, A.K., and M.J. Miller
44	Numerical experiments on the simulation of the 1979 Asian summer monsoon. (1984)	Mohanty, U.C., R.P. Pearce and M. Tiedtke
45	The effect of mechanical forcing on the formation of a mesoscale vortex. (1984)	Guo-xiong Wu and Shou-jun Chen
46	Cloud prediction in the ECMWF model. (1985)	Slingo, J., and B. Ritter

47	Impact of aircraft wind data on ECMWF analyses and forecasts during the FGGE period, 8-19 November. (1985)	Baede, A.P.M., P. Kållberg, and S. Uppala
48	A numerical case study of East Asian coastal cyclogenesis. (1985)	Chen, Shou-jun and L. Dell'Osso
49	A study of the predictability of the ECMWF operational forecast model in the tropics. (1985)	Kanamitsu, M.
50	On the development of orographic. (1985)	Radinović, D.
51	Climatology and systematic error of rainfall forecasts at ECMWF. (1985)	Molteni, F., and S. Tibaldi
52	Impact of modified physical processes on the tropical simulation in the ECMWF model. (1985)	Mohanty, U.C., J.M. Slingo and M. Tiedtke
53	The performance and systematic errors of the ECMWF tropical forecasts (1982-1984). (1985)	Heckley, W.A.
54	Finite element schemes for the vertical discretization of the ECMWF forecast model using linear elements. (1986)	Burridge, D.M., J. Steppeler, and R. Strüfing
55	Finite element schemes for the vertical discretization of the ECMWF forecast model using quadratic and cubic elements. (1986)	Steppeler, J.
56	Sensitivity of medium-range weather forecasts to the use of an envelope orography. (1986)	Jarraud, M., A.J. Simmons and M. Kanamitsu
57	Zonal diagnostics of the ECMWF operational analyses and forecasts. (1986)	Branković, Č.
58	An evaluation of the performance of the ECMWF operational forecasting system in analysing and forecasting tropical easterly disturbances. Part 1: Synoptic investigation. (1986)	Reed, R.J., A. Hollingsworth, W.A. Heckley and F. Delsol
59	Diabatic nonlinear normal mode initialisation for a spectral model with a hybrid vertical coordinate. (1987)	Wergen, W.
60	An evaluation of the performance of the ECMWF operational forecasting system in analysing and forecasting tropical easterly wave disturbances. Part 2: Spectral investigation. (1987)	Reed, R.J., E. Klinker and A. Hollingsworth
61	Empirical orthogonal function analysis in the zonal and eddy components of 500 mb height fields in the Northern extratropics. (1987)	Molteni, F.
62	Atmospheric effective angular momentum functions for 1986-1987. (1989)	Sakellarides, G.
63	A verification study of the global WAM model December 1987 - November 1988. (1989)	Zambresky, L.
64	Impact of a change of radiation transfer scheme in the ECMWF model. (1989)	Morcrette, J-J.
65	The ECMWF analysis-forecast system during AMEX. (1990)	Puri, K., P. Lönnberg and M. Miller
66	The calculation of geopotential and the pressure gradient in the ECMWF atmospheric model: Influence on the simulation of the polar atmosphere and on temperature analyses (1990)	Simmons, A.J. and Chen Jiabin
67	Assimilation of altimeter data in a global third generation wave model (1992)	Lionello, P., H. Günther and P. Janssen

68	Implementation of a third generation ocean wave model at the European Centre for Medium-Range Weather Forecasts (1992)	Günther, H., P. Lionello, P.A.E.M. Janssen et al.
69	A preliminary study of the impact of C-band scatterometer wind data on global scale numerical weather prediction (1992)	Hoffman, R.N.
70	Scientific assessment of the prospects for seasonal forecasting: a European perspective March 1993	Palmer, T.N. and D.L.T. Anderson
71	Results with a coupled wind-wave model February 1994	Janssen, P.A.E.M.
72	Implementation of the semi-Lagrangian method in a high resolution version of the ECMWF forecast model June 1994	Ritchie, H., C. Temperton, A. Simmons, M. Hortal, T. Davies, D. Dent and M. Hamrud
73	Raw HIRS/2 radiances and model simulations in the presence of clouds September 1994	Rizzi, R.
74	Ocean wave forecasting in the Mediterranean Sea. A verification study in the Spanish coastal zone. November 1994	Guillaume, A., M. Gomez Lahoz, B. Hansen and J.C. Carretero